

2

The theoretical foundations of gravitational waves: detection and emission

Simone Speziale¹ and Danièle Steer²

¹*Aix Marseille Univ., Univ. de Toulon, CNRS, CPT, UMR 7332, 13288
Marseille, France*

²*Laboratoire de Physique de l'ENS, Université Paris Cité, Ecole Normale
Supérieure, Université PSL, Sorbonne Université, CNRS, 75005 Paris*

In this chapter we focus on the detection and emission of GWs.

2.1. Detection of GWs

2.1.1. Coordinate displacements versus physical displacements

To study the effect of a gravitational wave, we consider a family of free-falling test masses. These follow time-like geodesics, whose tangent vector field u^μ satisfies the geodesic equation

$$u^\nu \text{NewA}_\nu u^\mu = \frac{du^\mu}{d\tau} + \Gamma_{\nu\rho}^\mu u^\nu u^\rho = 0, \quad u^\mu \partial_\mu = \frac{d}{d\tau}. \quad [2.1]$$

Here τ is the proper time τ , and $u^2 = -c^2$. If the masses are initially at rest, we have $u^a = 0$ and

$$\frac{du^\mu}{d\tau} = -\Gamma_{00}^\mu c^2 = \left(\frac{1}{2} \partial^\mu h_{00} - \partial_0 h_0^\mu \right) c^2. \quad [2.2]$$

The right-hand side vanishes if $h_{0\mu} = 0$, which as we have seen occurs for vacuum solutions in the TT gauge (and for any solution in the temporal gauge). Hence masses initially at rest will remain at rest at all times, and the coordinate distance as well as the coordinate time delay between two nearby time-like geodesics remains the same during the passage of the wave. This result provides us with an interpretation of the TT gauge: it is a choice of coordinates which are labelled by the position of test masses, just like the temporal gauge in the full theory is a choice of coordinates attached to free-falling observers. Now, even though the *coordinate distance* between two test masses remains the same in this gauge, their *physical distance* does not. It is given by

$$L = \int_0^{L_0} d\lambda \sqrt{g_{ab} \hat{e}^a \hat{e}^b} = \int_0^{L_0} d\lambda \left(1 + \frac{1}{2} h_{ab}^{\text{TT}} \hat{e}^a \hat{e}^b \right) + O(h^2). \quad [2.3]$$

Here \hat{e}^a is the tangent to the curve and λ an arbitrary parametrization thereof. To compare with the coordinate distance, let us choose \hat{e}^a to be constant along a coordinate axis, and take λ as coordinate. Then L_0 is the coordinate distance. It coincides with the physical distance in the background flat metric, but differs from it when the spacetime is perturbed. If we further assume that the wavelengths of the wave are much bigger than L_0 , we can ignore the space dependence of h_{ab}^{TT} and write the result as

$$L \simeq \left(1 + \frac{1}{2} h_{ab}^{\text{TT}} \hat{e}^a \hat{e}^b \right) L_0. \quad [2.4]$$

The approximation becomes of course exact if the direction of propagation of the wave is orthogonal to the axis connecting the masses.

The discussion offers an example of one of the most important lessons of general relativity, namely the importance of distinguishing coordinate effects from physical results. General covariance guarantees that all calculations can be performed in any coordinate system. But one has to always make sure that the physical consequences derived from the calculations are coordinate independent. In this example, we found that the trajectories of test particles are unaffected by the passage of the wave. This is a coordinate dependent statement, because the parametrization of the trajectories is coordinate-dependent. The relevant coordinate-independent quantity is the physical distance, and we found that it changes. In fact, it is easy to see that it would have changed in the same way in any coordinate system preserving the endpoints of the integral. In other words, the geodesic distance between two points physically identified is an observable. As we have already discussed, even though any coordinate system can be chosen, choosing a good coordinate system is important to simplify calculations. The fact that TT coordinates hide the passage of the wave may look like a negative feature, but it is in fact very convenient because it allows us to write the physical distance using fixed extrema in the integral at all times. The same effect is used when choosing the synchronous gauge in cosmology, it is often convenient to choose a coordinate system such that the values of the coordinate grid represent galaxies, so that their coordinate distance does not change, but the physical distance does.

The change of proper distance [2.4] also shows the meaning of the wave's polarizations. Using the example [1.84] of a monochromatic wave propagating along the z axis, and setting the test masses at $z = 0$, we can write the relative change in physical distance as

$$\frac{\delta L}{L_0} := \frac{L - L_0}{L_0} \simeq \left(\frac{1}{2} h_+ (\hat{e}^x \hat{e}^x - \hat{e}^y \hat{e}^y) + h_\times \hat{e}^x \hat{e}^y \right) \cos \omega t. \quad [2.5]$$

An h_+ polarization would cause pairs of masses along the x and y axis to periodically approach and recede, hence drawing a $+$ -like pulse in time, see Figure 2.1. An h_\times polarization would cause the same effect but along the axis $\hat{e}^a = (1, 1, 0)/\sqrt{2}$, namely rotated by 45 degrees. This type of deformation is also called 'shear' of the congruence of time-like geodesics followed by the test masses.

2.1.2. Gravitational waves and tidal forces

The quadrupolar nature of the gravitational force is evident from the shape of the tidal distribution of earth's oceans. The same type of tidal forces are

produced by the waves. To see this effect we look at the geodesic deviation equation. The analysis will also be useful to compare the description of the waves in two different coordinate systems. We recall that the geodesic deviation equation is given by

$$u^\rho \text{New}A_\rho(u^\nu \text{New}A_\nu \xi^\mu) = R^\mu{}_{\nu\rho\sigma} u^\nu u^\rho \xi^\sigma, \quad [2.6]$$

where ξ^μ is a vector connecting neighbouring geodesics, chosen such that $\xi \cdot u = [\xi, u] = 0$. At first order in h , and with the assumption of vanishing initial velocities, it reduces to

$$\frac{d^2 \xi^a}{dt^2} = -2\Gamma_{0\nu}^a u^0 \dot{\xi}^\nu - c^2 \xi^\nu \partial_\nu \Gamma_{00}^a. \quad [2.7]$$

In the TT gauge, the last term vanishes and the first one too if the initial velocity was zero. The coordinate distance between the geodesics stays constant, in agreement with the result already derived using the geodesic equation.

The description changes completely if we use a gauge corresponding to a local inertial frame, such as the Fermi normal coordinates, which can be used to set to zero the Christoffel symbols all along a chosen geodesic. As we see from [1.30], the metric only changes at quadratic order in the coordinate distance from the origin, hence coordinate distances coincide with physical distance at first order. In this local inertial frame gauge, the first term of [2.7] vanishes but not the second, which furthermore matches the lowest order of the Riemann tensor. Hence we have

$$\frac{d^2 \xi^a}{dt^2} = c^2 R^a{}_{00b} \xi^b = \frac{1}{2} \ddot{h}_{\text{TT}}^{ab} \xi_b, \quad [2.8]$$

where in the second equality we have neglected any contribution from the potentials. Hence if we have a detector that can detect tidal effects, it will be sourced precisely by the physical components of the GW, and not by the gauge ones. At first order in h , the geodesic deviation equation [2.8] is solved by

$$\xi^a(t) = \xi^a(0) + \frac{1}{2} h_{\text{TT}}^{ab} \xi_b(0). \quad [2.9]$$

Since in this gauge the coordinate distance coincides with the physical distance at first order, we recover the gauge-invariant result [2.4] but where this time the metric is unchanged, and it is the extremum of the integral that has moved. The equation [2.9] can be used to visualize the physical effect of the

passage of the wave. To that end, we consider a circular distribution of test masses centered around the origin in the plane perpendicular to the direction of propagation of the wave, see Fig. 2.1. Then we can identify the displacement vector with the coordinate vector of each mass (labelled by i), and the effect of a monochromatic wave of frequency ω is

$$\begin{aligned} x_i(t) &= x_i(0) + h_+(t)x_i(0) + h_\times(t)y_i(0), \\ y_i(t) &= y_i(0) - h_+(t)y_i(0) + h_\times(t)x_i(0). \end{aligned}$$

The effect is shown in Fig. 2.1, where the period $T = 2\pi/\omega$.

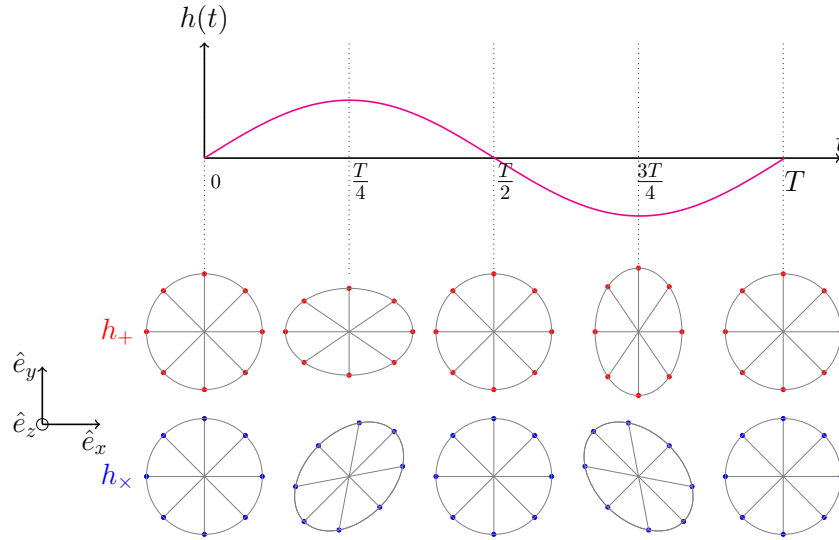


Figure 2.1: The effect of the two polarizations on a circular distribution of test masses. In the upper panel (red circles) $h_+ \neq 0$ and $h_\times = 0$. The lower panel has $h_\times \neq 0$ and $h_+ = 0$.

If external forces are present, on top of the gravitational one, then [2.1] and [2.6] acquire additional terms on the right hand side. So in particular [2.8] now reads

$$\frac{d^2 \xi^a}{dt^2} = c^2 R^a{}_{00b} \xi^b + \frac{F^a}{m}. \quad [2.10]$$

as an example, consider a material bar. While the effect of the gravitational wave is to stretch spacetime changing the physical distance between the

molecules of the bar, there are also electromagnetic forces that hold the bar together, and which are intrinsically much stronger. For instance, the Coulomb interaction between two electrons one angstrom apart is $\sim 10^{42}$ times stronger than its Newtonian counterpart. For this reason, one could in principle use simply a rigid ruler measuring the distance between two freely falling masses to detect gravitational waves. The problem with this is the weakness of the waves, which requires one to set up more sophisticated experiments.

A special cases of external forces appearing on the right-hand side of [2.10] are the inertial forces. These, by the equivalence principle, can be reabsorbed in a coordinate transformation of the metric. For instance if the frame has both an acceleration \vec{a} and an angular velocity $\vec{\Omega}$ with respect to a local inertial frame, then (Ni and Zimmermann 1978)

$$\begin{aligned} ds^2 = & -c^2 dt^2 \left(\left(1 + \frac{1}{c^2} \vec{a} \cdot \vec{x}\right)^2 - \frac{1}{c^2} (\vec{\Omega} \times \vec{x})^2 + R_{0c0d} x^c x^d \right) \\ & + 2cdtdx^a \left(\frac{1}{c} \epsilon_{abc} \Omega^b x^c - \frac{2}{3} R_{0cad} x^c x^d \right) + dx^a dx^b \left(\delta_{ab} - \frac{1}{3} R_{acbd} x^c x^d \right) \\ & + O(x^2), \end{aligned} \quad [2.11]$$

and [2.10] becomes

$$\frac{d^2 \vec{\xi}}{dt^2} = -\vec{a} - 2\vec{\Omega} \times \vec{v} + \frac{\vec{F}}{m} + O(x^2). \quad [2.12]$$

All the gravitational effects as well as further non-inertial effects such as centrifugal acceleration are $O(x^2)$. So in order to be capable of detecting gravitational waves, a detector must first of all be freed from all the external forces that would otherwise drown the signal in noise.

In realistic physical systems, the emission will not be a plane wave, but rather a wave packet with finite temporal extension. The effect on the circular distribution will then be a superposition of different frequencies and different helicities, each with their own (time-dependent) amplitude. The temporal finiteness of the signal can also lead to a new type of effect: after the wave has passed, the distribution will stop oscillating, but its shape will in general not be the same as before the wave's arrival. This effect is called displacement memory, and we will see below in Sec.2.4.5 an explicit example. The effect carries the memory of the wave, since it permits in principle to detect the passage of a gravitational wave even after the event. In practise though the detection is very difficult, because the external forces that make up the matter distribution will act and bring it back to its rest configuration. It is nonetheless one of the targets of future detectors (Grant and Nichols 2023).

2.1.3. Interferometers

Let us briefly describe how the formulas above are used in the most common type of detectors, laser interferometers. Other chapters in this collection will cover more details as well as the types of detectors. The basic idea of a laser interferometer is to detect physical changes like [2.3] from the time-of-flight of monochromatic light signals. This can be done easily in the linear theory if we make the additional approximations that gravitational potentials can be neglected,¹ and that the wavelength of the signal is much longer than the arms of the interferometer. The first approximation guarantees that the only source of curvature comes from the wave, hence the Riemann tensor scales like λ^{-2} . We can then set up a free falling frame say in Fermi normal coordinates centered on the beam splitter's geodesic. Thanks to the second approximation, the spatial projection of the null geodesics follows straight lines, hence the time of flight is directly related to the physical distance along the interferometer's arms. The latter is given by [2.4] regardless of the direction of the wave, thanks again to the assumption that the wavelength is much larger than the arms' length. Denoting $\hat{e}_{1,2}^a$ the two axis, we have

$$L_2 - L_1 = \frac{L_0}{2} h_{ab}^{\text{TT}} (\hat{e}_1^a \hat{e}_1^b - \hat{e}_2^a \hat{e}_2^b). \quad [2.13]$$

For a typical signal $h \sim 10^{-21}$ (see overview Section 1.1.4), hence the difference in arrival time would be $\Delta T = (L_2 - L_1)/c \sim 10^{-26} s$ which is way too small to be measurable. Two ingenious ideas come to the rescue. First, Michelson-Morley's idea to measure not time but phase interferences, and two increasing the effective path of light through Fabry-Perot cavities.

If we set the lasers so that the phases at the beam splitter are identical, the phase shift after the travel to and back from the mirrors will be

$$\Delta\phi = \frac{2\pi\nu}{c} N_p (2L_1 - 2L_2), \quad [2.14]$$

where $N_p = 1$ for a Michelson device and up to 300 for the Fabry-Pérot one used in Ligo/Virgo. Plugging in the previous result we arrive at

$$\Delta\phi = \frac{2\pi\nu}{c} N_p L_0 h_{ab}^{\text{TT}} (\hat{e}_1^a \hat{e}_1^b - \hat{e}_2^a \hat{e}_2^b), \quad [2.15]$$

1. The potentials generated by the source can be naturally neglected because they fall off faster than the radiative modes, so this approximation concerns mostly the local gravitational field.

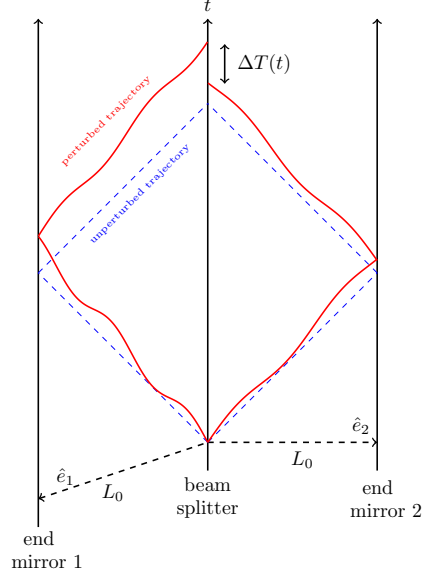


Figure 2.2: World lines of photon trajectories between the beam splitter and the end mirrors in an interferometer with arms of equal length. Blue dashed lines: with no gravitational wave. Red lines: perturbed trajectories. In the long wavelength approximation $\lambda \gg L_0$ the red lines are straight (but still have different angles than the unperturbed blue lines), and $\Delta T = 2\Delta L/c$.

where now \hat{e}^a are the unit vectors giving the direction of each arm.

It is possible to express the result in terms of the two wave polarizations, if we introduce a rotation from $R(\theta, \varphi) := R_z(\varphi)R_y(\theta)$ from the detector's frame to the frame of propagation, plus a reflection to take into account the fact that the axis of propagation is opposite to the direction of the source acting also on y to keep right-handed orientation of the frame. The result is

$$\Delta\phi = \frac{4\pi\nu}{c} N_p L_0 (F_+ h_+ + F_\times h_\times), \quad [2.16]$$

where the coefficients

$$F_+ = \frac{1}{2}(1 + \cos^2 \theta) \cos 2\varphi, \quad F_\times = \cos \theta \sin 2\varphi \quad [2.17]$$

are called detector's pattern functions.² This shows that while a single two-armed interferometer is sensitive to both polarizations, it cannot distinguish them. It also shows that the sensitivity depends on the relative orientation with respect to the sources. The dependence is very strong, to the point that there are directions in which the detector is completely blind, like $(\theta, \varphi) = (\frac{\pi}{2}, \frac{\pi}{4})$. Hence the importance of multiple detectors in order to increase sensitivity in every direction and the possibility of distinguishing the polarizations. Multiple detectors also allow studying the localization of the source via triangulation.

If the approximation $\lambda \gg L_0$ is no longer valid, then one has to take into account the redshift changes during the time of flight, see for instance discussion in (Andersson 2019).

2.2. Generation of GWs from sources

2.2.1. Introducing sources

Following the principle of general covariance, the matter Lagrangian should satisfy the property [1.23], namely be written solely in terms of the dynamical matter fields and spacetime metric, and no additional background fields. The simplest way to obtain a viable matter Lagrangian is then to start from the one used in the absence of gravity, and 'covariantize' it by the replacements

$$\eta_{\mu\nu} \rightarrow g_{\mu\nu}, \quad \partial_\mu \rightarrow \text{NewA}_\mu, \quad d^4x \rightarrow \sqrt{-g}d^4x. \quad [2.18]$$

Doing so introduces a minimal coupling of matter to the gravitational field. Additional interactions can be included if phenomenologically or theoretically motivated, provided they respect [1.23].³ Having done so, we define the matter energy-momentum tensor

$$T_{\mu\nu} = -\frac{2c}{\sqrt{-g}} \frac{\delta \mathcal{L}_M}{\delta g^{\mu\nu}}. \quad [2.19]$$

Inserting this definition in [1.23], and using [1.20], we obtain

$$\xi_\nu \text{NewA}_\mu T^{\mu\nu} + \partial_\mu (\xi^\mu \mathcal{L}_M - T^{\mu\nu} \xi_\nu) = \frac{1}{\sqrt{-g}} E_\psi \delta_\xi \psi \quad [2.20]$$

2. This formula can be generalize to include an additional angle between the polarization basis, as well as a non-perpendicular angle between the arms.

3. Or not, if one is considering modified theories of gravity.

where we recall that ψ denotes the matter fields and E_ψ the matter field Euler-Lagrange equations. On solutions of the matter field equations $E_\psi = 0$, and since the equation holds for any ξ , we conclude that

$$\text{NewA}_\mu T^{\mu\nu} = 0 \quad [2.21]$$

in the absence of boundaries. This equation replaces the familiar conservation of the energy-momentum tensor guaranteed by Noether's theorem in flat space-time. More precisely, the Noether current of the total Lagrangian $\mathcal{L}_{\text{EH}} + \mathcal{L}_{\text{M}}$ is

$$j_\xi^\mu = \frac{c^3}{8\pi G} \left(E^\mu{}_\nu \xi^\nu - \text{NewA}_\nu \text{NewA}^{[\mu} \xi^{\nu]} \right), \quad [2.22]$$

where E are Einstein's equations [1.16], namely [1.24] with the vacuum equations replaced by the equations in the presence of matter), and whose conservation requires to be on-shell of both the Einstein's and matter's field equations:

$$\text{NewA}_\mu j_\xi^\mu = \frac{c^3}{8\pi G} E^{\mu\nu} \text{NewA}_\mu \xi_\nu - \frac{1}{c} \text{NewA}_\mu T^{\mu\nu} \xi_\nu \hat{=} 0. \quad [2.23]$$

Even though [2.21] is often referred to as the general covariant version of energy-momentum conservation, it is important to remark that it is *not* a conservation equation in the usual sense. To understand this point, let us follow the usual procedure to obtain Noether charges from the current, and apply Stokes's theorem to a finite region M with boundary ∂M . To do so we need a scalar, which we obtain by contracting the left-hand side of [2.21] with a vector ξ^μ . After integrating by parts, we find

$$\begin{aligned} \int_M \text{NewA}_\mu T^{\mu\nu} \xi_\nu \sqrt{-g} d^4x &= \oint_{\partial M} T^{\mu\nu} \xi_\nu n_\mu \sqrt{q} d^3y \\ &+ \int_M T^{\mu\nu} \text{NewA}_\mu \xi_\nu \sqrt{-g} d^4x, \end{aligned} \quad [2.24]$$

where we denoted by n_μ the normal and by y the coordinates of ∂M . If $\text{NewA}_{(\mu} \xi_{\nu)}$ vanishes, namely if the Killing equations is satisfied, then [2.21] can be turned into a conservation law. To do so, we consider the case in which ∂M consists of two space-like hypersurfaces Σ_1 and Σ_2 connected by a time-like boundary \mathcal{T} , see Fig.2.3. If the fields satisfy conservative boundary conditions at \mathcal{T} (typically \mathcal{T} asymptotically far away and fall-off conditions on the fields), then

$$Q_\xi := \int_{\Sigma_1} T^{\mu\nu} \xi_\nu n_\mu \sqrt{q} d^3y = \int_{\Sigma_2} T^{\mu\nu} \xi_\nu n_\mu \sqrt{q} d^3y \quad [2.25]$$

for each Killing vector ξ . Therefore [2.21] gives as many conserved quantities as there are isometries in spacetime. For flat spacetime, these are the ten Poincaré charges. For a generic dynamical spacetime, there are none.

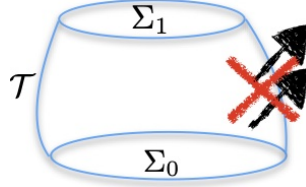


Figure 2.3: A region of spacetime bounded by two space-like hypersurfaces $\Sigma_{1,2}$ and a time-like one \mathcal{T} . With conservative boundary conditions on \mathcal{T} , [2.25] establishes as many conservation laws as there are Killing vectors.

The validity of [2.21] implies the matter equations of motion, as we have seen from its derivation. In particular, if matter consists of test particles, namely free motion without self-interaction and ignoring the back-reaction on the metric, this equation implies the geodesics equation in curved spacetime. This is for instance how one can derive the relativistic corrections to the Kepler problem, by evaluating [2.21] on the Schwarzschild background. At lowest order in the weak-field expansion [1.46], [2.21] reduces to the energy-momentum conservation law in flat spacetime,

$$\partial_\mu T^{\mu\nu} = 0. \quad [2.26]$$

This means that at lowest order the matter can interact with itself, but not with the gravitational field: the sources follow geodesics in flat spacetime (that is, straight lines). To include the effect of gravity on the sources we must go beyond the lowest order. In other words, the linearized theory still describes gravity in the Newtonian way, namely as a force acting in flat spacetime. Of course, it already contains departures from Newton's theory, since it includes the special relativistic effects such as the gravito-magnetic interaction and radiation.

2.2.2. Source multipoles

Let us study the conserved quantities [2.25] that arise on the Minkowski background. We choose Σ to be a global hypersurface of constant time t , write its unit normal as $n_\mu = -\partial_\mu t$, and the ξ' are the ten Poincaré Killing vectors

[1.48]. We can thus identify ten conserved quantities corresponding to energy and momentum

$$c^2 M := \int d^3x T^{00}, \quad cP^a := \int d^3x T^{0a}, \quad [2.27]$$

which correspond to taking $a^\mu{}_\nu = 0$ and unit values of b^μ , and relativistic angular momentum

$$cL^a = \frac{c}{2} \epsilon^a{}_{bc} L^{bc} := \epsilon^a{}_{bc} \int d^3x x^b T^{0c},$$

$$c^2 K^a := \int d^3x (T^{0a} ct - T^{00} x^a), \quad [2.28]$$

which correspond to taking $b^\mu = 0$ and unit values of $a^a{}_\nu$ and $a^0{}_\nu$ respectively. Their conservation can be easily checked. We start by separating [2.26] in time and space components,

$$c^{-1} \dot{T}^{00} + \partial_a T^{a0} = 0, \quad c^{-1} \dot{T}^{0a} + \partial_b T^{ab} = 0. \quad [2.29]$$

Then using Stokes' theorem and vanishing boundary conditions we immediately see that

$$\dot{M} = \dot{P}^a = \dot{L}^a = \dot{K}^a = 0. \quad [2.30]$$

While the first of [2.27] is the the total energy, we followed the custom in the literature to denote it M and refer to it as 'mass', using Newtonian language. The first of [2.28] is the angular momentum with respect to the frame defined by $n_\mu = -\partial_\mu t$. The second conserved quantity can be rewritten as $K^a = I^a - tP^a$, where we introduce the center-of-mass position

$$I^a = \frac{1}{c^2} \int d^3x T^{00} x^a. \quad [2.31]$$

Conservation of K^a is thus the statement that the center of mass moves following the total momentum.

The conserved quantities can be used to fix a reference frame as follows. First, we can choose the center-of-mass frame, in which $P^a = 0$. This removes

the freedom of Lorentz boosts. Then, we can fix the origin to be in the center-of-mass, which removes the freedom of spatial translations⁴. The rotation freedom can be fixed choosing the axis so that L^a has only one component (say z), and the remaining $\text{SO}(2)$ freedom is fixed choosing an axis in the plane perpendicular to L^a . Finally the time translation symmetry is fixed setting the zero value of the clock.

The quantity I^a is also called mass-dipole moment. The terminology comes about if we see $\rho = c^{-2}T_{00}$ as a distribution, then I^a is the first moment of that distribution. Following this logic, we introduce a multi-index notation for the higher multipole moments:

$$\begin{aligned} I^{ab\dots} &= \frac{1}{c^2} \int d^3x T^{00} x^a x^b \dots, & P^{a,b\dots} &= \frac{1}{c} \int d^3x T^{0a} x^b \dots, \\ S^{ab,c\dots} &= \int d^3x T^{ab} x^c \dots \end{aligned} \quad [2.32]$$

The conservation laws [2.29] together with integration by parts in the absence of boundary terms provide relations between multipole moments and time variations of higher multipoles, such as

$$\begin{aligned} P^a &= -\dot{I}^a, & S^{ab} &= \frac{1}{2}\ddot{I}^{ab}, \\ \dot{S}^{ab,c} &= \frac{1}{6}\ddot{I}^{abc} + \frac{1}{3}(\ddot{P}^{a,bc} + P^{b,ac} - P^{c,ab}), & \dot{P}^{a,b} &= S^{ab} \end{aligned} \quad [2.33]$$

and so on. The first one above is the conservation of K^a already seen, and relates the momentum monopole to the mass dipole time variation. The second one allows one to determine the total effect of the stresses in the matter in terms of the second time derivative of the mass quadrupole. These relations are useful because it is typically easier to measure and interpret the multipole moments of the mass and momentum distributions, rather than the spatial stresses.

When working with multipoles, it is typically convenient to organize them into irreducible representations of the rotation group, which are labeled by an integer number l and have $2l + 1$ components each, as recalled earlier. This can be achieved expanding the distribution in spherical harmonics, e.g.

4. Sometimes the two operations are referred collectively as ‘center-of-mass frame’, something they are separated with the first one alone being called ‘center-of-momentum’ frame.

$\rho = \sum_{l,m} \rho_{l,m} Y_{l,m}$, then the integrals of the modes $\rho_{l,m}$ are the irreducible multipoles. It is possible although more cumbersome to do this composition directly in Cartesian coordinates without introducing spherical harmonics. One then gets

$$M = \frac{1}{c^2} \int d^3x \rho, \quad D^a = I^a = \frac{1}{c^2} \int d^3x \rho x^a, \quad [2.34]$$

$$Q^{ab} = \frac{1}{c^2} \int d^3x \rho (x^a x^b - \frac{r^2}{3} \delta^{ab}), \quad O^{abc} = \frac{1}{c^2} \int d^3x \rho (15x^a x^b x^c - 9x^{(a} \delta^{bc)} r^2), \quad [2.35]$$

and so on.

2.2.3. Solving the wave equation with sources

We are interested in the emission of gravitational waves from matter sources, without incoming radiation. This can be imposed choosing the retarded Green function and setting to zero the independent degrees of freedom $h_{\mu\nu}^{\text{OTT}}$. The general solution is then

$$\begin{aligned} \bar{h}_{\mu\nu} &= -\frac{16\pi G}{c^4} \int d^4x' G(x, x') T_{\mu\nu}(x') \\ &= \frac{4G}{c^4} \int d^3x' \frac{T_{\mu\nu}(t - \frac{1}{c}|\vec{x} - \vec{x}'|, \vec{x}')}{|\vec{x} - \vec{x}'|}. \end{aligned} \quad [2.36]$$

using [1.145] and the specialized De Donder gauge with no homogeneous solution. Even in the linearized approximation, the integral is in general very complicated and there is no analytic solution. So we resort to approximation schemes. In particular, we introduce two independent approximations:

- (i) Wave-zone approximation: we assume to be very far away from the sources, that is $R := |\vec{x}| \gg |\vec{x}'|$. This allows us to expand the integrand in powers of $1/R \ll 1$. For the numerator, we have

$$|\vec{x} - \vec{x}'| = R - \vec{N} \cdot \vec{x}' + \dots \quad [2.37]$$

where $\vec{N} := \vec{x}/R$, and

$$T_{\mu\nu}(t - \frac{1}{c}|\vec{x} - \vec{x}'|, \vec{x}') \simeq T_{\mu\nu}(t_{\text{R}}, \vec{x}') + \frac{\vec{N} \cdot \vec{x}'}{c} \dot{T}_{\mu\nu}(t_{\text{R}}, \vec{x}') + \dots, [2.38]$$

where we introduce the *retarded time*⁵

$$t_{\text{R}} := t - \frac{R}{c}. \quad [2.39]$$

For the denominator, we have

$$\frac{1}{|\vec{x} - \vec{x}'|} = \frac{1}{R} + \frac{\vec{N} \cdot \vec{x}'}{R^2} + \frac{3}{2}(x'_a x'_b - \frac{r'^2}{3} \delta_{ab}) \frac{N^a N^b}{R^3} + \dots \quad [2.40]$$

Furthermore, the direction of propagation of the wave coincides with the direction from the source, namely $-\vec{N}$ if we take the origin of the coordinates inside the source. Hence the TT projector can be written in terms of \vec{N} instead of the wave vector.

- (ii) Slow dynamics: We assume that the dynamics of the source is slow, so that time derivatives in [2.38] are small corrections. To understand why, consider that the integration coordinate \vec{x}' spans at most the size of the source, and if this has a typical frequency scale ω_s (for instance in a binary, the frequency of the orbit), then $v_s := |\vec{x}'| \omega_s$ is the velocity scale of the source. It follows that

$$\frac{|\vec{x}'|}{c} \dot{T}_{\mu\nu} \sim \frac{|\vec{x}'| \omega_s}{c} T_{\mu\nu} \sim \frac{v_s}{c} T_{\mu\nu} \quad [2.41]$$

is suppressed by v/c . The Taylor expansion [2.38] is therefore controlled by the parameter $v/c \ll 1$, and it is called post-Newtonian expansion.

The approximated solution can thus be written as

$$\bar{h}_{\mu\nu}(x) = \frac{4G}{c^4 R} \int d^3 x' \left(T_{\mu\nu}(t_{\text{R}}, \vec{x}') + \frac{N_a}{c} \dot{T}_{\mu\nu}(t_{\text{R}}, \vec{x}') x'^a + \frac{N_a}{R} T_{\mu\nu}(t_{\text{R}}, \vec{x}') x'^a + \dots \right) \quad [2.42]$$

The first term is the leading order; the second term is the first of the PN corrections; the third term is the first of the $1/R$ corrections. Using the multipole definitions [2.32] and their conservation laws [2.33], we can rewrite the different components of the solution [2.42] as

5. Namely the time at which a signal travelling at the speed of light was sent in order to arrive at t .

$$\bar{h}_{00} = \frac{4G}{c^2 R} \left(M - \frac{N^a}{c} P_a + \frac{N^a N^b}{2c^2} \ddot{I}_{ab} + \frac{N^a}{R} \dot{I}_a + \dots \right) \Big|_{t_R}, \quad [2.43a]$$

$$\bar{h}_{0a} = -\frac{4G}{c^3 R} \left(P_a + \frac{N^b}{2c} \ddot{I}_{ab} + \frac{N^b}{2RC} (L_{ab} + \dot{I}_{ab}) + \dots \right) \Big|_{t_R}, \quad [2.43b]$$

$$\bar{h}_{ab} = \frac{4G}{c^4 R} \left(\frac{1}{2} \ddot{I}_{ab} + \frac{N^c}{3c} \left(\frac{1}{2} \ddot{I}_{abc} + \ddot{P}_{a,bc} + \ddot{P}_{b,ac} - \ddot{P}_{c,ab} \right) + \dots \right) \Big|_{t_R}. \quad [2.43c]$$

These are the first few terms of the double expansion in velocities and distance from the sources. Notice that we are not giving all metric components to the same higher order; this is because our goal here is just to give a qualitative understanding of how the expansion works. Furthermore which orders are dominant depends on the type of question asked.

The lowest order of the time-time component reproduces the Newtonian result.⁶ The first PN correction is the movement of the source, and can always be set to zero by going to the rest frame. Doing so eliminates the lowest order of the \bar{h}_{0a} component. The first corrections in that component contain the gravitomagnetic effects relevant to the Lense-Thirring effect, for instance. Notice also that the angular momentum is sub-leading in R , as one could have expected from a large distance expansion of Kerr's metric.

The radiative degrees of freedom are in the spatial components [2.43c] and can be extracted acting with the projector [1.88]. We have the mass quadrupole at leading order, and the first PN correction features the mass octupole and momentum quadrupole. We can immediately remark the absence of monopole and dipole contributions to the emission of waves. This is a direct consequence of the conservation laws, since they imply that the mass monopole and dipole

6. This result may look unfamiliar, since the Schwarzschild metric in static coordinates differs from it by a factor of 2. But recall that our analysis assumes De Donder gauge – otherwise [2.36] would not be the right solution –, aka harmonic gauge. The Schwarzschild metric in harmonic gauge reads

$$ds^2 = -\frac{\rho - r_s/2}{\rho + r_s/2} dt^2 + \frac{\rho + r_s/2}{\rho - r_s/2} d\rho^2 + (\rho + r_s/2)^2 d\Omega, \quad \rho = r - r_s/2,$$

and then

$$h_{00} = \frac{2M}{\rho}, \quad h_{rr} = \frac{2M}{\rho}, \quad h_{AB} = 2M\rho h_{AB}^{s^2}, \quad h = -h_{00} + h_{aa} = \frac{4M}{\rho}. \quad [2.44]$$

So the factor 4 instead of 2 is because we are in traceless gauge, which is not the usual coordinates in which we write the metric.

have vanishing second time derivatives. As a consequence, an oscillating spherical distribution would not emit gravitational waves, in agreement with Birkhoff theorem in the full theory, nor would a distribution with axial symmetry rotating at constant velocity, in agreement with Kerr's solution.

Applying the TT projector removes any trace, hence $h^{\text{TT}} = \bar{h}^{\text{TT}}$ and one can replace I_{ab} with the irreducible quadrupole moment Q_{ab} , and obtain at lowest order

$$h_{ab}^{\text{TT}}(t, \vec{x}) = \frac{2G}{c^4 R} \ddot{Q}_{ab}^{\text{TT}}(t_{\text{R}}). \quad [2.45]$$

This is the celebrated *first quadrupole formula*, derived by Einstein in 1918: The dominant radiation in the slow-motion approximation arises from the acceleration of the quadrupole moment of the mass distribution. From this we can also obtain the expressions for the two independent polarizations. If $\vec{k} = \hat{z}$, we can use [1.71a] and

$$h_{+}(t, r) = \frac{G}{c^4 R} (\ddot{Q}_{11} - \ddot{Q}_{22})|_{t_{\text{R}}}, \quad h_{\times} = \frac{2G}{c^4 R} \ddot{Q}_{12}|_{t_{\text{R}}}. \quad [2.46]$$

For a general \vec{k} it is obtained replacing $h_{ab} \rightarrow (G/c^4 R)Q_{ab}$ in [1.91]. Notice also that $P^{\text{TT}}(Q) = P^{\text{TT}}(I)$ since the projector removes the trace, hence we can replace Q_{ab} with I_{ab} in these expressions.

Let us make some order-of-magnitude estimates. By dimensional analysis, the mass multipoles scale like Mr^l , where r is the typical size of the source. If the dynamics of the system has a typical velocity scale v , then $Q \sim Mr^2$ and $\ddot{Q} \sim Mv^2$. This gives

$$h \sim \frac{G}{c^4 R} Mv^2 = 5 \times 10^{-19} \left(\frac{M}{10M_{\odot}} \right) \left(\frac{1\text{Mpc}}{R} \right) \frac{v^2}{c^2}. \quad [2.47]$$

For example, two 10-solar-masses black holes at merger will have a fully relativistic speed $v \sim c$, which gives a 10^{-18} amplitude at galactic distances, and 10^{-21} at 100 Mpc where the Virgo cluster is located.

This estimate is the lowest order of various approximations, which is useful to recap here: (1) weak-field, PM expansion; (2) long-distance, multipolar expansion; (3) small velocities, PN expansion. To obtain more accurate results, one has to include higher order corrections. Doing so is actually far from simple. Not only we have three different expansion parameters with non-trivial hierarchies among them, we also have to face both technical and conceptual

challenges. Let us list a few, and tools used to deal with them. The PN expansion is not a convergent series, but rather what is known as an asymptotic series. Its accuracy degrades as we increase R . Dealing with this mathematical problem requires techniques such as the matched asymptotic expansion. Related to this is also the more conceptual issue that the causal propagation determined by the Green's function at lowest order follows the null cones of the background Minkowski metric. But null cones are bent by the gravitational interaction, hence higher order corrections have to also modify the retarded time to the correct one. For instance for the Schwarzschild metric the correct retarded time is

$$\begin{aligned} u &= t - R/c - 2GM/c^2 \ln(R - 2GM/c^2) \\ &= t_{\text{r}} + \frac{2GM}{c^2} \ln R - \left(\frac{2GM}{c^2}\right)^2 \frac{1}{R} + O(R^{-2}). \end{aligned}$$

Hence higher orders change the notion of retarded time. Another tricky effect comes in at higher orders: the waves backscatter and self-interact, causing a delay in part of the signal, which starts travelling inside the light-cone, similar to light slowing down in a medium due to interactions with the medium. Then the total signal includes a 'tail' that comes after the main part of the signal. To take this into account one has to include effects that arise from integration over time.

Another problem is divergences appear after the first iteration, because convolution of Poisson integrals diverge even if the initial source has compact support. To regularize this unphysical divergence one has to split the integrals into near-zone and far-zone integrations. These and other types of difficulties plagued the theory throughout most of the seventies, and were addressed thanks to the work of many brilliant researchers, including pioneers like Thorne, Will, and Damour. On the phenomenological side, people thought for a while that the lowest quadrupole order would have been enough to match experiments, given the weakness of the waves. Later theoretical work, e.g. the seminal paper (Cutler *et al.* 1993), clarified the observational sensitivity to the PN corrections and justified the importance of the endeavour. The task is very challenging, and researchers have come up with different approaches. We refer to the specialized literature (Thorne 1980 ; Blanchet 2006 ; Poisson and Will 2014 ; Goldberger and Rothstein 2006) for reviews of this more advanced topic. In the following we will content ourselves to stay at lowest order, which is enough to understand the basics of the physics, if not for a detailed match to observations.

2.3. Flux-balance laws

2.3.1. Energy of gravitational waves

A consequence of the equivalence principle and diffeomorphism invariance is that there cannot be any local tensorial quantity that fully describes gravitational energy.⁷ For instance, the Hamiltonian one finds from the Legendre transform of the Lagrangian is a sum of constraints, and thus identically zero when evaluated on solutions. Any attempt to work around these facts and define quasi-local observables representing the gravitational energy unavoidably run into trouble with ambiguities and dependence on coordinates or other unphysical background structures (Szabados 2009). The clearest well-defined resolution to this problem is to work with global notions of energy. Such global notions are useful to describe isolated systems, namely spacetimes that are fully dynamical in a certain region, but become well approximated by flat spacetime at large distances from this region. In this case, one can introduce a physically meaningful notion of boundary to the spacetime, and exploit the fact that the Hamiltonian picks up a boundary contribution which is non-vanishing on solutions. The resulting *surface charges* can be used to characterise the total energy momentum and angular momentum of the system, and can be derived as Noether charges as well. Examples of this construction are the ADM charges at spatial infinity, and the BMS charges at future null infinity, as mentioned in Sec. 1.2.2.

The difficulties in defining gravitational energy arise already at the linearized level, as we are about to see. Let us look at the gravitational wave perturbation simply as a spin-2 field propagating on the Minkowski background. Thanks to the Poincaré invariance of the background, we can apply Noether's theorem and derive a conserved energy-momentum tensor for $h_{\mu\nu}$. An explicit calculation starting from the linearized Lagrangian gives

$$t_{\mu\nu}^N = \frac{c^4}{32\pi G} \left(\partial_\mu h^{\alpha\beta} \partial_\nu h_{\alpha\beta} - \frac{1}{2} \eta_{\mu\nu} \partial_\lambda h_{\rho\sigma} \partial^\lambda h^{\rho\sigma} \right), \quad [2.48]$$

where the label N stands for Noether, and we assumed here the De Donder condition to simplify the expression. This tensor is conserved, namely $\partial_\mu t^{N\mu\nu} \doteq 0$, but has no clear physical meaning, because it is *not* gauge-invariant: It changes under a linearized diffeomorphism [1.50], and consequently assigns a non-zero

7. Such quantity will have to be zero in a local free-falling frame where the effects of gravity are absent, and if it were a tensor, it would then be zero in any frame. A tensorial quantity capturing *some* aspects of gravitational energy can be constructed using the Bel-Robinson tensor, but it is fourth-order in derivatives, therefore does not have the right physical dimensions, and will capture only higher-order terms of the gravitational energy.

value of energy-momentum to pure gauge modes. Furthermore, we can make it vanish entirely at any point using Riemann normal coordinates, since in these coordinates the first derivatives of the metric vanish at that point. Maybe one can exploit the freedom in the Noether construction to find a better quantity? Noether currents are not unique after all, and defined only up to adding total derivatives whose conservation is trivial. In the case at hand, the ambiguity is the freedom to add terms with the structure

$$t_{\mu\nu}^N + \partial^\rho \partial^\sigma U_{\mu\rho\nu\sigma}, \quad [2.49]$$

where U has the same index symmetries as the Riemann tensor. One may hope that there exists a representative in the equivalence class [2.49] that would be gauge invariant, but this is not the case: the lack of gauge-invariance is a direct consequence of the equivalence principle, and this impacts already the linearized theory.⁸

While looking at global quantities such as the surface charges mentioned at the beginning of the section is the safest way to define energy in the full theory, the perturbative treatment offers an alternative, ‘quasi-local’ possibility. It is possible to construct quasi-local gauge-invariant quantities by introducing a spacetime averaging procedure based on the properties of the background. We consider a region L whose size is much larger than the typical wavelength λ of the perturbation, but much smaller than the typical wavelength λ_B of the background (which is infinite for a flat background), and we define $\langle F \rangle = \frac{1}{L} \int_L F$. If applied to an expression quadratic in the Fourier modes like [2.48], the procedure suppresses combinations with different frequencies or different phases, in a way completely similar to how the total energy in a standard background-dependent theory comes mainly from positive interference superposition of waves. The difference is that in background-dependent theories averaging the energy is a choice, since the local energy density is theoretically also well defined. In gravity it is not a choice but mandatory, since there is no meaningful local energy density, and furthermore care is needed to define correctly the procedure in a way to make it compatible with general covariance. Detailed analysis (Isaacson 1968 ; Burnett 1989) shows that the result of the

8. It is instructive to put this problem in perspective with what happens in the electromagnetic case. If one computes the canonical energy-momentum tensor of Maxwell’s theory using the Noether formula, one also finds a meaningless gauge-dependent expression. However, the Noether construction only defines the tensor up to total divergences, and it is possible to find one that gives a gauge-invariant expression, and which is furthermore symmetric and coincides with the one derived from the variation with respect to the metric. In gravity there is an analogue problem, but even adding total divergences it is not possible to find a local gauge invariant quantity.

procedure is that expressions under the averaging sign can be freely integrated by parts in space and, upon going on-shell, also in time derivatives since a wave propagates on the light-cone. For instance,

$$\langle \partial_\mu h_{\alpha\beta} \partial^\mu h^{\alpha\beta} \rangle = -\langle h_{\alpha\beta} \square h^{\alpha\beta} \rangle = 0 \quad [2.50]$$

outside the sources. Under this procedure, we find

$$\langle t_{\mu\nu}^N \rangle = \frac{c^4}{32\pi G} \langle \partial_\mu h^{\alpha\beta} \partial_\nu h_{\alpha\beta} \rangle. \quad [2.51]$$

One can show that the averaging procedure makes the right-hand side gauge-invariant (Isaacson 1968). This means that it can be expressed in terms of the TT projection and the gauge invariant potentials. The latter can be neglected if the sources variation (induced by the partial derivatives in the expression above) occurs over much longer time scales than the h^{TT} wavelengths.⁹ This motivates the definition of

$$t_{\mu\nu} := \frac{c^4}{32\pi G} \partial_\mu h_{\text{TT}}^{ab} \partial_\nu h_{ab}^{\text{TT}}, \quad t_{\mu\nu} = \langle t_{\mu\nu}^N \rangle. \quad [2.52]$$

This quantity is actually gauge-invariant at lowest order, since the only non-invariant terms are the partial derivatives, and these transform linearly in $\xi \sim O(h)$. It follows that in so far as lowest order results are needed, we can forget about the averaging procedure, and use [2.52]. To get fully gauge-invariant results, we should average, or look at scalar quantities built out of $t_{\mu\nu}$ integrated over the whole spacetime, which automatically include the averaging and produce gauge-invariant results. An intermediate situation concerns integration over a whole space-like hypersurface. These are invariant under spatial diffeomorphisms, but not time diffeomorphisms. Hence one would get a gauge-invariant result at lowest order, and time averaging is needed to remove the gauge-dependency in the short time scales.

The expression [2.52] is the one used by Einstein to determine the energy carried away by gravitational waves. It is conserved (outside the sources) and gauge independent, hence a valid quantity for the task. It has however a limited applicability: first, it relies heavily on the special background chosen, and had we worked with a non-isometric one, then there would be no Noether charge

9. In (Poisson and Will 2014) this step is called short-wave approximation, and it is performed without the averaging, in the context of the Landau-Lifshitz approach described in Appendix 2.7.

to begin with. Second, it is not clear how to extend this construction to treat higher orders in perturbation theory. These shortcomings can be addressed if we look at the actual back-reaction on the metric caused by the waves. In fact the actual "effective" source that determines the second-order metric perturbation is not [2.48], but rather the second order expansion of the Einstein tensor, as we saw in [1.36]. The candidate gravitational energy-momentum tensor $t_{\mu\nu}^G$ obtained in this way is also conserved. In fact, an explicit calculation shows that it differs from [2.48] precisely by a term like [2.49], with U a certain quadratic expression in derivatives of $h_{\mu\nu}$.

The second candidate $t_{\mu\nu}^G$ for a definition of energy-momentum tensor of gravitational waves has the better property that it depends on second derivatives of the metric, so it cannot be made to vanish at any given point. However, it is still not gauge-invariant. Therefore one has to invoke again the averaging procedure. Upon doing so, one finds that the two prescriptions give a consistent answer (Isaacson 1968):

$$\langle t_{\mu\nu}^G \rangle = \langle t_{\mu\nu}^N \rangle = \langle t_{\mu\nu} \rangle. \quad [2.53]$$

This is reassuring that averaging offers a viable way to extract unambiguous and gauge-independent quantities. The prescription t^G overcomes some limitations of the Einstein-Noether construction. It can be used in perturbation theory around an arbitrary background, and can be systematically extended to any order in perturbation theory, by computing higher order corrections $G_{\mu\nu}^{(n)}$ and evaluating them on the perturbed solution. Notice however that the procedure of interpreting a piece of the field equations as source on the right-hand side is by itself ambiguous, because it relies on a choice of dynamical field. For instance, if we organize the higher order corrections as an expansion in the trace-reversed perturbation $\bar{h}_{\mu\nu}$ as opposed to $h_{\mu\nu}$, we would get different expressions for $G_{\mu\nu}^{(n)}$.

In this context, a convenient approach to the perturbative expansion around Minkowski is given by the Landau-Lifshitz reformulation of Einstein's equations. This gives a third candidate for energy-momentum, known as Landau-Lifshitz pseudo-tensor, whose lowest order differs from the previous two options again by a term like [2.49]. The Landau-Lifshitz pseudo-tensor has the usual problems, in particular gauge-dependence and vanishing at any point in a local inertial frame, but once again provides the gauge-invariant result after averaging:

$$\langle t_{\mu\nu}^{LL} \rangle = \langle t_{\mu\nu} \rangle. \quad [2.54]$$

Even if coordinate-dependent, this approach has the merit of being set up in a way that makes it very natural to develop a systematic perturbative expansion, since the pseudo-tensor is defined already at non-perturbative level, and

does not need to be calculated order by order as in the previous approach. Furthermore, it provides a prescription for the energy, momentum and angular momentum as surface charges that, even though restricted in validity to Cartesian coordinates in the region far away from the sources, can be evaluated including higher orders, and bypasses the need for the spatial averaging of volume integrals. For these reasons, the Landau-Lifshitz formulation is widely used by the community working in the post-Newtonian expansion. We review it briefly in Appendix 2.7.

We have restricted the discussion to energy and energy-momentum, but similar considerations apply also to define the angular momentum of gravitational waves. In this case, the result of the averaging procedure starting from any of the three prescriptions described above motivates the following definition (DeWitt 2011 ; Thorne 1980 ; Poisson and Will 2014)

$$j^a := \frac{1}{2} \epsilon^a{}_{bc} j^{bc} = -\frac{c^4}{32\pi G} \epsilon^{abc} (\dot{h}_{de}^{\text{TT}} x_b \partial_c h_{\text{TT}}^{de} + 2\dot{h}_{bd}^{\text{TT}} h_{cd}^{\text{TT}}). \quad [2.55]$$

As before, this gives a gauge-invariant quantity after global integration or averaging.

Averaging provides gauge invariant quasi-local quantities at lowest order in perturbation theory. This is satisfactory from a conceptual point of view, and to gain a first handle on how to describe physical processes involving gravitational waves. However, it is not a very practical tool, especially if one wants to go beyond the lowest order, and set up a systematic perturbative expansion. In this context, it is again easier to work with gauge-fixed quantities at all intermediate steps, and then extract only at the end the physical predictions in terms of gauge-invariant observables. For instance, there is no problem in working with the non-averaged notions of energy-momentum and angular momentum, as long as one does not attempt to give them a direct physical interpretation.¹⁰ The idea is to use them to perform calculations, and at the end read off the physical dynamics not from their evolution but from that of gauge-invariant quantities such as the amplitude and frequency of TT modes, or the evolution of relative distances such as the periastron of an orbit. We will see this approach explicitly below.

10. As mentioned at the beginning of the section, a direct physical interpretation is on the other hand possible in terms of asymptotic global quantities such as ADM and BMS charges.

2.3.2. Dissipation equations

The fact that [2.52] is conserved means that we can derive identities between time and spatial derivatives like those that led to the conservation laws [2.30] for the matter sources. The key difference however is that the matter sources had compact support, hence we could neglect boundary contributions when integrating by parts. This is no longer true for the gravitational contributions, since the waves have non-compact support. The non-vanishing of the boundary terms has the effect that the ‘charges’ corresponding to energy, momentum and angular momentum are no longer conserved. This dissipation is precisely the statement that gravitational waves carry energy and have a physical impact on the system.

In practise, we do not even need to use the conservation equation in order to study the dissipation, because of a special property of the explicit solution [2.43]. Each metric component has functional dependence on coordinate of the form $f(t_R, N^a)$. For such functions, it is easy to check that

$$\partial_a f = -\frac{N_a}{c} \dot{f} + O(R^{-1}). \quad [2.56]$$

The leading order of this approximation plays an important role in simplifying many formulas in the wave zone, where $R \gg 1$.

Let us begin our analysis from the flux of gravitational energy, namely the emitted power. This is given by

$$\frac{dE}{dt} = \int_{\Sigma} \dot{t}^{00} d^3x = -c \oint_{\partial\Sigma} t^{0a} N_a dS = \frac{c^4}{32\pi G} \oint_{\partial\Sigma} \dot{h}_{cd}^{\text{TT}} N^a \partial_a h_{\text{TT}}^{cd} dS, \quad [2.57]$$

Stokes theorem choosing as boundary a 2-sphere of radius R in the asymptotic region (hence the outgoing unit normal is simply N_a , and $dS = R^2 d^2\Omega$ where $d^2\Omega = \sin\theta d\theta d\phi$) and [2.52] in the last equality. The spatial derivative can be replaced at lowest order with a time derivative using again [2.56], and we arrive at

$$\frac{dE}{dt} = -\frac{c^3}{32\pi G} \oint_{\partial\Sigma} \dot{h}_{ab}^{\text{TT}} \dot{h}_{\text{TT}}^{ab} dS = -\frac{G}{8\pi c^5 R^2} \oint_{\partial\Sigma} \ddot{Q}_{ab}^{\text{TT}} \ddot{Q}_{\text{TT}}^{ab} dS, \quad [2.58]$$

where in the last step we used the explicit form [2.43] of the solution, in particular [2.45]. To evaluate the integral, we observe that the only angular dependence occurs in the TT projector [1.88]. Using the following formula,

$$\oint_{S^2} P^{\text{TT}cd}_{ab} d^2\Omega = \frac{8\pi}{5} \left(\delta_{(a}^c \delta_{b)}^d - \frac{1}{3} \delta_{ab} \delta^{cd} \right), \quad [2.59]$$

we find

$$\frac{dE}{dt} = -\frac{G}{5c^5} \ddot{Q}_{ab} \ddot{Q}^{ab} |_{t_R}. \quad [2.60]$$

This is the second famous quadrupole formula of Einstein (Einstein 1918). It gives the instantaneous power radiated at a distance R from the source and a time t , as a function of the quadrupole time variation at the retarded time $t - R$. There are two important remarks to make about this equation. First, after integration the index contraction occurs over all indices of the (traceless) quadrupole moment, thanks to the right-hand side of [2.59]. Second, as explained in the previous Section, the instantaneous power so defined is *not* observable, because of its gauge-dependence, only its time average over scales larger than the waves' wavelength is. To get some numerical estimates from the formula we just derived, let us consider [1.84] with $h_{\times} = 0$, then

$$t_{tt}^{\text{eff}} = \frac{\omega^2 h_+}{2\kappa^2} = 1.5 \frac{mW}{m^2} \left(\frac{h_+}{10^{-22}} \right)^2 \left(\frac{f}{1\text{kHz}} \right)^2. \quad [2.61]$$

For the linear momentum,

$$\begin{aligned} \frac{dP^a}{dt} &= \frac{1}{c} \int_{\Sigma} \dot{t}^{0a} d^3x = - \int_{\Sigma} \partial_b t^{ab} d^3x \\ &= - \oint_{\partial\Sigma} t^{ab} N_b dS = - \frac{c^2}{32\pi G} \oint_{\partial\Sigma} N^a \dot{h}_{cd}^{\text{TT}} \dot{h}_{\text{TT}}^{cd} dS, \end{aligned} \quad [2.62]$$

where we used twice [2.56] in the last equality. Since N^a is an odd function on the sphere, the integral vanishes: there is no loss of momentum at lowest order, namely at order G/c^5 . A change in the total momentum of the system caused by the emission of GWs ('kick') occurs only at the next order G/c^7 , when mixing of multipoles of different parity occurs.

For the angular momentum flux we obtain

$$j^a = \int_{\Sigma} d^3x \partial_t j^a = -\frac{1}{c} \oint_{\partial\Sigma} j^a dS \frac{c^3}{16\pi G} \epsilon^{abc} \oint_{\partial\Sigma} (\dot{h}_{de}^{\text{TT}} x_b \partial_c h_{\text{TT}}^{de} + 2\dot{h}_{bd}^{\text{TT}} h_c^{\text{TT}d}) dS. \quad [2.63]$$

Using the quadrupole formula [2.45] and performing the integrals using identities similar to [2.59], one arrives at

$$j^a = -\frac{2G}{5c^5} \epsilon^{abc} \ddot{Q}_{bd} \ddot{Q}_c^d |_{t_R}. \quad [2.64]$$

Angular momentum loss occurs at the same order as energy loss, and involves one lesser time derivative.

2.4. GWs from binary systems: elliptical, circular and hyperbolic orbits

We now apply the results of the previous section to determine the GW signal from binary systems. We will first consider the case of a bound system, with circular or elliptical orbits. These provide a simple yet realistic model of astrophysical sources that corresponds to the signals observed by LVK. We will see how one can express the two quadrupole formulas (and more generally the dissipation equations) in terms of the dynamics of the sources, compute the backreaction leading to orbital decay and increased wave emission, and produce analytic waveforms. We will also see explicitly the importance of the averaging procedure, which in the case of bound binary systems neatly separates the effects related to the two time-scales involved: the period of each orbit, and the ‘secular’ effects that cumulate over many orbits. We will then consider the case of unbounded, hyperbolic orbits, produce their waveforms. These orbits are interesting because they provide the simplest examples of displacement memory and gravitational capture.

2.4.1. Newtonian equations

We first recall the Newtonian equations of motion for two non-spinning point-particles of masses $m_{1,2}$, with relative position $\vec{r} = \vec{x}_1 - \vec{x}_2$ and relative velocity $\vec{v} = \vec{v}_1 - \vec{v}_2$. Coordinates are chosen such that binary is in the (x, y) plane. The two time-dependent unit vectors \vec{n} and $\vec{\lambda}$ are defined by

$$\vec{r} = r\vec{n}, \quad \dot{\vec{n}} = (\dot{r}\vec{n} - r\dot{\psi}\vec{\lambda}), \quad [2.65]$$

$$\vec{v} = \dot{r}\vec{n} + r\dot{\psi}\vec{\lambda}, \quad \dot{\vec{\lambda}} = (-\dot{\psi}\vec{n} - \psi\dot{\lambda}), \quad [2.66]$$

where $\psi = \psi(t)$. The observer/detector is at position $\vec{R} = R\vec{N}$ where in spherical polar coordinates the unit vector $\vec{N} = (\sin\varphi\cos\theta, \sin\varphi\sin\theta, \cos\varphi)$, see figure 2.4. Newton’s equations in the centre of mass (CM) frame are

$$r(\psi) = \frac{p}{1 + e\cos(\psi)}, \quad [2.67]$$

$$\dot{\psi} = \sqrt{\frac{Gm}{p^3}}(1 + e\cos(\psi))^2 \quad [2.68]$$

where $m = m_1 + m_2$ the total mass and p is semi-latus rectum. It follows from Eqs. [2.65]-[2.68] that

$$\vec{v} = \sqrt{\frac{Gm}{p}}(-\sin\psi, e + \cos\psi, 0). \quad [2.69]$$

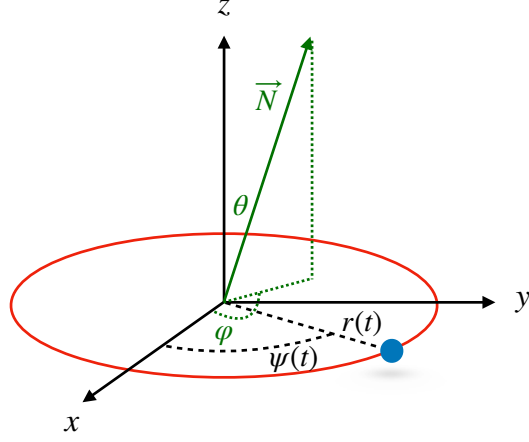


Figure 2.4: Bound binary system in the centre of mass frame: basic quantities and angles

and

$$\frac{|\vec{v}|^2}{c^2} = \left(\frac{Gm}{c^2 p} \right) (1 + e^2 + 2e \cos \psi). \quad [2.70]$$

The Newtonian approximation requires $\vec{v}^2 \ll c^2$, and thus the dimensionless ratio $Gm/c^2 p \ll 1$. The conserved angular momentum of the orbits, $\vec{L} = L\vec{e}_z$, is given by

$$L = \nu \sqrt{Gmp} \quad [2.71]$$

where ν is the dimensionless mass ratio

$$\nu = \frac{m_1 m_2}{m^2}. \quad [2.72]$$

The total conserved orbital energy is

$$E = \nu \frac{Gm^2}{2p} (e^2 - 1). \quad [2.73]$$

Bound systems the eccentricity $e < 1$, while unbound ones have $e > 1$.

- **Elliptical Orbits** have $0 < e < 1$ with $-\pi \leq \psi < \pi$, $r_{\min} = p/(1+e)$ and $r_{\max} = p/(1-e)$. The orbital angular frequency ω_0 and period T are given by Keplers laws, namely

$$\omega_0 = \sqrt{\frac{Gm(1-e^2)^3}{p^3}} \quad \text{and} \quad T = \frac{2\pi}{\omega_0} \quad [2.74]$$

- **Circular orbits** have $e = 0$ and radius $r = p$, and orbital frequency and period given by Eq. [2.74].
- **Hyperbolic orbits** have $e > 1$. Now $\psi_-(e) \leq \psi < \psi_+(e)$ where

$$\psi_{\pm} = \pm \cos^{-1}(1/e), \quad [2.75]$$

and correspondingly $\sin \phi_{\pm} = \pm e^{-1} \sqrt{e^2 - 1}$. These orbits are not periodic, but have a characteristic time-scale (a burst time scale) related to the characteristic frequency scale

$$\omega_c = \sqrt{\frac{Gm(e^2 - 1)^3}{p^3}}. \quad [2.76]$$

The closest distance of approach $r_{\min} = p/(1+e)$ at $\psi = 0$. As $\psi \rightarrow \psi_{\pm}$, $v \rightarrow v_{\infty}$ with

$$\frac{v_{\infty}^2}{c^2} = \frac{Gm}{c^2 p} (e^2 - 1). \quad [2.77]$$

Of course GR effects modify these Newtonian equations of motion, but consistently with the approximation scheme discussed in Section 1.3 they are not included here. Thus for example we ignore precession, namely that over an orbital period the perihelion of elliptical orbits advances by $\Delta_e = 2\pi(3Gm/c^2 p)$, while for hyperbolic orbits $\Delta_h = (\Delta_e/3) \{6 \arccos(-1/e) + e^{-2} \sqrt{e^2 - 1} [2(2 + e^2) + 5\nu(e^2 - 1)]\}$, see e.g. (Damour and Deruelle 1985).

2.4.2. *Waveform, energy and angular momentum fluxes*

In the quadrupole approximation, the TT component of the waveform is given by Eq. [2.45], or equivalently rewriting the traceless quadrupole tensor $Q_{ij} = I_{ij} - \frac{1}{3}I\delta_{ij}$ in terms of the quadrupole moment I_{ij} ,

$$h_{cd}^{\text{TT}}(t, \vec{R}) = \frac{2G}{c^4 R} P^{\text{TT}ab}(\vec{N}) \ddot{I}_{ab}(t_{\text{R}}) \quad [2.78]$$

where $t_{\text{r}} = t - R/c$ is the retarded time. At large distances $R \gg p$ relative to the source, the projection tensor onto the TT components is given by Eq. [1.87].

Substituting Eqs. [2.67] and [2.68] into the definition of the quadrupole tensor [2.32] gives

$$I_{ab} = \nu m r_a r_b. \quad [2.79]$$

Then using Newtonian's equations of motion $d\vec{v}/dt = -Gm\vec{n}/r^2$ it follows that

$$\dot{I}_{ab} = 2\nu m \left(v_a v_b - \frac{Gm}{r} n_a n_b \right). \quad [2.80]$$

Thus from Eqs. [2.65] and [2.69] the non-zero components of \ddot{I}_{ab} are

$$\ddot{I}_{11} = -2\nu m c^2 \left(\frac{Gm}{c^2 p} \right) [\cos(2\psi) + e \cos^3 \psi], \quad [2.81]$$

$$\ddot{I}_{12} = -2\nu m c^2 \left(\frac{Gm}{c^2 p} \right) [\sin(2\psi) + e \sin \psi (1 + \cos^2 \psi)], \quad [2.82]$$

$$\ddot{I}_{22} = 2\nu m c^2 \left(\frac{Gm}{c^2 p} \right) [\cos(2\psi) + e \cos \psi (1 + \cos^2 \psi) + e^2], \quad [2.83]$$

with \ddot{I}_{ab} having the dimensions of energy. The third derivatives of the quadrupole tensor are straightforwardly obtained from Eq. [2.83] and [2.68] and read

$$\dddot{I}_{11} = 2\nu(m c^2) \frac{c}{p} \left(\frac{Gm}{c^2 p} \right)^{3/2} (1 + e \cos \psi)^2 [2 \sin(2\psi) + 3e \cos^2 \psi \sin \psi] \quad [2.84]$$

$$\dddot{I}_{12} = 2\nu(m c^2) \frac{c}{p} \left(\frac{Gm}{c^2 p} \right)^{3/2} (1 + e \cos \psi)^2 [-2 \cos(2\psi) + e \cos \psi (1 - 3 \cos^2 \psi)] \quad [2.85]$$

$$\dddot{I}_{22} = -2\nu(m c^2) \frac{c}{p} \left(\frac{Gm}{c^2 p} \right)^{3/2} (1 + e \cos \psi)^2 [2 \sin(2\psi) + e \sin \psi (1 + 3 \cos^2 \psi)]. \quad [2.86]$$

The GW perturbation is given by substituting these expressions into Eq. [2.78]. In the direction $\vec{N} = \hat{z}$ the plus and cross polarisations are given

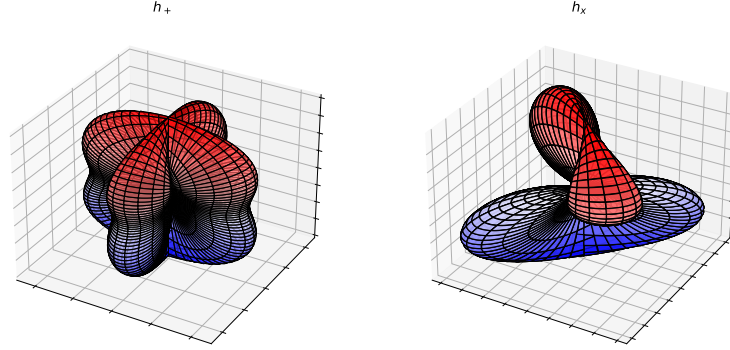


Figure 2.5: Surfaces of constant h_+ and h_\times polarisations for circular orbits $e = 0$. Here we have chosen $\psi = \pi$.

by (see Eq. [2.46]),

$$h_+(t) = \frac{G}{c^4 R} (\ddot{I}_{11} - \ddot{I}_{22}) = -h_0 [2 \cos(2\psi) + e \cos \psi + 2e \cos^3 \psi + e^2] \Big|_{t_R} \quad [2.87]$$

$$h_\times(t) = \frac{2G}{c^4 R} \ddot{I}_{12} = -2h_0 [\sin(2\psi) + e \sin \psi (1 + \cos^2 \psi)] \Big|_{t_R}. \quad [2.88]$$

where the dimensionless amplitude is

$$h_0 = 2\nu \left(\frac{Gm}{c^2 R} \right) \left(\frac{Gm}{c^2 p} \right). \quad [2.89]$$

The time-dependence is determined from $\psi(t)$ which is a solution of Eq. [2.68]. In a similar way, $h_{+,\times}(t, \theta, \varphi)$ for any $\vec{N} = (\sin \varphi \cos \theta, \sin \varphi \sin \theta, \cos \varphi)$ can be deduced from Eq. [1.91]. Figure 2.5 shows surfaces of constant $h_{+,\times}$ as a function of (θ, φ) , for a fixed value of $\psi = \pi$ and $e = 0$. The quadrupolar nature is clearly visible.

In the limit of circular orbits ($e = 0$), only the terms in $\cos(2\psi)$ and $\sin(2\psi)$ remain, and furthermore $\psi = \omega_0 t$ from Eq. [2.68]. Thus for circular orbits, the GW frequency is twice the orbital frequency $f = 2\omega_0$. Figure 2.6 shows the waveforms as a function of retarded time, in units of T , for 2.5 orbital periods. Below we will determine the frequency dependence when $e \neq 0$.

In the quadrupole approximation, the energy and angular momentum fluxes are given by (see Eqs. [2.60] and [2.64])

$$P_{\text{GW}}(\psi) = \frac{G}{5c^5} \ddot{Q}_{ab} \ddot{Q}^{ab} = \frac{2G}{15c^5} \left[\ddot{I}_{11}^2 + \ddot{I}_{22}^2 + 3\ddot{I}_{12}\ddot{I}_{12} - \ddot{I}_{11}\ddot{I}_{22} \right] \quad [2.90]$$

$$J_{\text{GW}}^z(\psi) = \frac{2G}{5c^5} \epsilon^{3k\ell} \ddot{I}_{ka} \ddot{I}_{\ell a} = \frac{2G}{5c^5} \left[(\ddot{I}_{11} - \ddot{I}_{12}) \ddot{I}_{12} + \ddot{I}_{12} (\ddot{I}_{22} - \ddot{I}_{11}) \right] \quad [2.91]$$

(only the z -component of angular momentum is relevant since the binary is in the xy -plane). Substituting Eq. [2.86] gives

$$P_{\text{GW}}(\psi(t)) = P_{\text{GW}}^{e=0} (1 + e \cos \psi)^4 \left[1 + 2e \cos \psi + \frac{e^2}{12} (1 + 11 \cos^2 \psi) \right] \Big|_{t_{\text{R}}} \quad [2.92]$$

$$J_{\text{GW}}^z(\psi(t)) = J_{\text{GW}}^{e=0} (1 + e \cos \psi)^3 \left[1 + \frac{3}{2} e \cos \psi - \frac{e^2}{4} (1 - 3 \cos^2 \psi) \right] \Big|_{t_{\text{R}}} \quad [2.93]$$

where for circular orbits the constant rates of emission are given in terms of the dimensionless coefficient $Gm/c^2 p$ by

$$P_{\text{GW}}^{e=0} = \frac{32}{5} \nu^2 \left(\frac{c^5}{G} \right) \left(\frac{Gm}{c^2 p} \right)^5 \quad [2.94]$$

$$J_{\text{GW}}^{e=0} = \frac{32}{5} \nu^2 (mc^2) \left(\frac{Gm}{c^2 p} \right)^{7/2} \quad [2.95]$$

The above expressions are valid for all $e \geq 0$ provided $\bar{v}^2 \ll c^2$. Figure 2.6 shows the waveforms Eq. [2.87]-[2.88] and power emitted Eq. [2.92] over 2.5 periods of a circular orbit with $e = 0$, in unit of t_{R}/T where T is the orbital period. Figure 2.7 shows the same for an elliptical orbit with $e = 0.3$. In both cases the periodic motion is clear. Over a longer time-scales $t \gg T$, however, the emission of energy and angular momentum backreact on the orbital trajectories and must be considered. For a hyperbolic orbit, the corresponding plots are given in figure 2.8. The motion is obviously no-longer periodic and simply amounts to a fly-by: thus backreaction effects do not accumulate over time and will be less significant (see subsection 2.4.5).

We now evaluate the effect of energy and angular momentum dissipation on the waveforms (for elliptical, circular and hyperbolic orbits in turn).

2.4.3. Elliptical and circular orbits: backreaction effects

The effect of the emitted GW radiation (energy and angular momentum) produce a radiation-reaction force, whose backreaction on the Newtonian gravitational attraction between the bodies in the binary system perturbs their

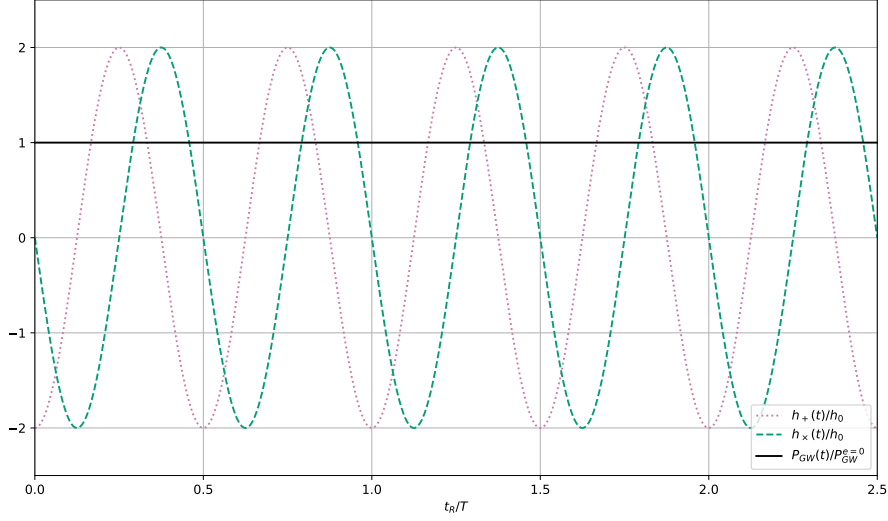


Figure 2.6: Circular orbits. The plot shows h_+ and h_\times polarisations, and emitted GW power (solid line), as a function of retarded time in units of T for 2.5 orbital periods. The emitted power is constant and given by Eq. [2.94]. The GW wavelength is $cT/2$.

dynamics. On time-scales $t \gg T$ these secular effects can be calculated by writing the conservation equations in averaged form

$$\frac{dE}{dt} = -\langle P_{\text{GW}} \rangle \quad \frac{dL}{dt} = -\langle J_{\text{GW}} \rangle \quad [2.96]$$

where E and L are the orbital angular energy and angular momentum given in Eqs. [2.73] and [2.71], and the average is over one orbital period:

$$\langle X \rangle = \frac{1}{T} \int_0^T dt X(t) = \frac{1}{T} \int_{-\pi}^{\pi} d\psi \frac{1}{\dot{\psi}} X(\psi), \quad [2.97]$$

where $\dot{\psi}$ is given in Eq. [2.68]. The aim of this subsection is to solve these equations to determine the secular evolution of $e(t)$, $p(t)$, and thus $h_{+,\times}(t)$ with backreaction included.

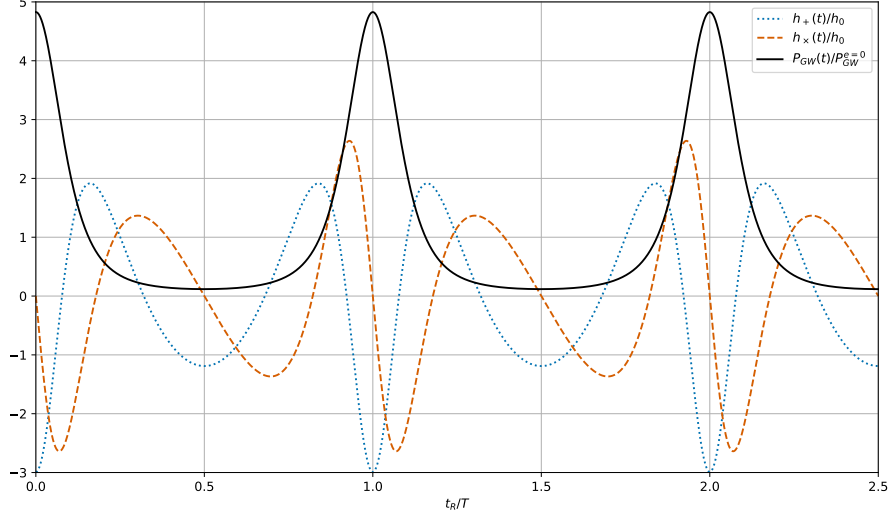


Figure 2.7: Elliptical orbit with $e = 0.3$. The plot shows that h_+ and h_\times polarisations, and emitted GW power, as a function of retarded time in units of T for 2.5 orbital periods. The emitted power is largest at $\psi = 0 \bmod 2\pi$ where the orbital velocity is the largest.

2.4.3.1. Averaged Energy and momentum radiation

The averaged GW energy and angular momentum radiation are straightforward to calculate. For the GW energy

$$\langle P_{\text{GW}} \rangle = \frac{1}{T} \int_{-\pi}^{\pi} d\psi \frac{1}{\psi} P_{\text{GW}}(\psi), \quad [2.98]$$

and substituting [2.92] leads directly to the *Peter and Mathews* formula (Peters and Mathews 1963):

$$\langle P_{\text{GW}} \rangle = P_{\text{GW}}^{e=0} (1 - e^2)^{3/2} \left[1 + \frac{73}{24}e^2 + \frac{37}{96}e^4 \right]. \quad [2.99]$$

(This expression is only valid for $e < 1$ as we are dealing with elliptical orbits.) Keeping p constant, the radiation increases from $e = 0$, to a maximum at $e \sim 0.5$ before decreasing and vanishing at $e = 1$. The averaged angular momentum radiation is similarly determined using [2.93] and gives

$$\langle J_{\text{GW}} \rangle = j_{\text{GW}}^{e=0} (1 - e^2)^{3/2} \left[1 + \frac{7}{8}e^2 \right]. \quad [2.100]$$

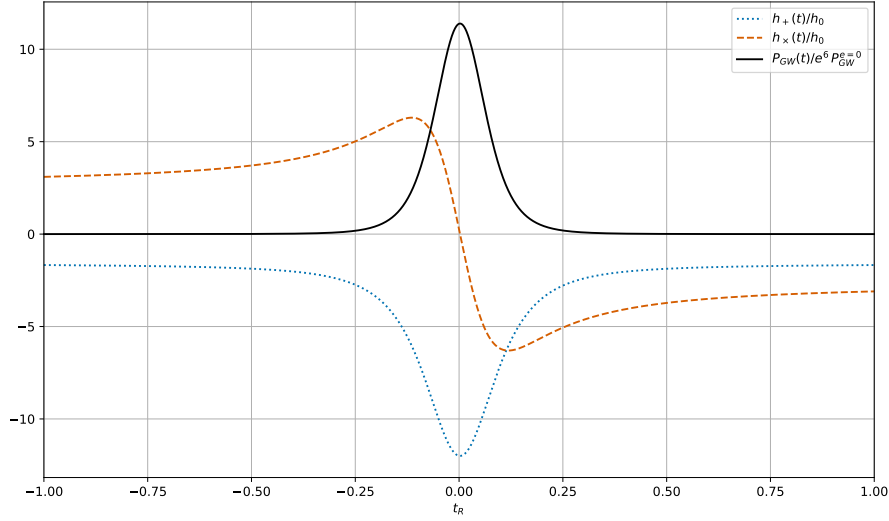


Figure 2.8: Hyperbolic orbits with $e = 2$. The h_+ and h_\times polarisations and emitted GW power as a function of retarded time, for an initial value $\psi = \psi_-$ see Eq. [2.75]. The motion is no-longer periodic and a burst of GW energy emitted when $\psi = 0$ at $t = 0$. Note that the emitted power scales as e^6 for large e , see Eq. [2.92], and for that reason in the plot the power is normalised by an extra factor of e^6 . See section 2.4.5

2.4.3.2. Elliptical orbits: frequency content

Before solving [2.96], we discuss the frequency the emitted GWs. For circular orbits, as mentioned above, the emitted GWs have frequency which is twice the orbital frequency $\omega_0 = \sqrt{Gm/p^3}$. When $e < 1$, other harmonics of $\omega_0 = \sqrt{Gm(1-e^2)^3/p^3}$ are excited, as is clear from figure 2.7. The time average radiated power $\langle P_{\text{GW}} \rangle$ given in [2.98] is determined by the third time derivative of the quadrupole tensor which itself can be decomposed into a Fourier series

$$I_{ij}(t) = \nu m p^2 \left\{ \tilde{A}_{ij}^{(0)} + \sum_{n=1}^{\infty} \left[\tilde{A}_{ij}^{(n)} \cos(n\omega_0 t) + \tilde{B}_{ij}^{(n)} \sin(n\omega_0 t) \right] \right\} \quad [2.101]$$

with $\tilde{A}_{ij}^{(0)} = \frac{1}{\nu m p^2 T} \int_0^T dt I_{ij}(t)$, $\tilde{A}_{ij}^{(n)} = \frac{2}{\nu m p^2 T} \int_0^T dt I_{ij}(t) \cos(\omega_0 n t)$, $\tilde{B}_{ij}^{(n)} = \frac{2}{\nu m p^2 T} \int_0^T dt I_{ij}(t) \sin(\omega_0 n t)$. The components of $I_{ij}(t)$ are nothing other than

the x and y coordinates of the particle which are real and given by the components of \vec{r} in [2.65], from which one finds see e.g. (Maggiore 2007)

$$0 = \tilde{B}_{11}^{(n)} = \tilde{A}_{12}^{(0)} = \tilde{A}_{12}^{(n)} = \tilde{B}_{22}^{(n)}, \quad \tilde{A}_{11}^{(0)} = \frac{1+4e^2}{2}, \quad \tilde{A}_{22}^{(0)} = \frac{1}{2} \quad [2.102]$$

and

$$\tilde{A}_{11}^{(n)} = \frac{1}{(1-e^2)^2} \cdot \frac{1}{n} [J_{n-2}(ne) - J_{n+2}(ne) - 2e(J_{n-1}(ne) - J_{n+1}(ne))], \quad [2.103]$$

$$\tilde{B}_{12}^{(n)} = \frac{1}{(1-e^2)^{3/2}} \cdot \frac{1}{n} [J_{n+2}(ne) + J_{n-2}(ne) - e(J_{n+1}(ne) + J_{n-1}(ne))] \quad [2.104]$$

$$\tilde{A}_{22}^{(n)} = \frac{1}{(1-e^2)} \cdot \frac{1}{n} [J_{n+2}(ne) - J_{n-2}(ne)] \quad [2.105]$$

Then $\ddot{I}_{ij}(t)$ are obtained directly from Eq. [2.101] with the time derivatives lead to factors of $n^3\omega_0^3$. Substituting into [2.90] and then taking *time average* to calculate $\langle P_{\text{GW}} \rangle$ leads to terms such as $\langle \sin n\omega_0 t \sin m\omega_0 t \rangle \sim \delta_{mn}$ meaning that the different harmonics do not interfere. In conclusion one finds

$$\langle P_{\text{GW}} \rangle = \sum_{n=1}^{\infty} \langle P_n \rangle \quad [2.106]$$

where

$$\langle P_n \rangle = P_{\text{GW}}^{e=0} \cdot \frac{n^6}{96} (1-e^2)^4 \left[\left(\tilde{A}_{11}^{(n)} \right)^2 + \left(\tilde{B}_{12}^{(n)} \right)^2 + 3 \left(\tilde{A}_{22}^{(n)} \right)^2 - \tilde{A}_{11}^{(n)} \tilde{B}_{12}^{(n)} \right]. \quad [2.107]$$

where $P_{\text{GW}}^{e=0}$ is given in Eq. [2.94]. The $\langle P_n \rangle$ are plotted in figure 2.9 for different values of e . The quadrupolar nature of the radiation for $e = 0$ (red) is again clear since all the GW power is emitted into the $n = 2$ mode. Power is radiated into more harmonics as e increases, and the frequency at which maximum power is radiated also increases with e .

2.4.3.3. Waveform with dissipation

We now return to Eqs. [2.96], where on the left hand side the time-dependence is in $e(t)$ and $p(t)$. By definition, see [2.71], $L = \nu\sqrt{Gmp}$ from which

$$\frac{dL}{dt} = \frac{\nu c}{2} \sqrt{\frac{Gm}{c^2 p}} \frac{dp}{dt}. \quad [2.108]$$

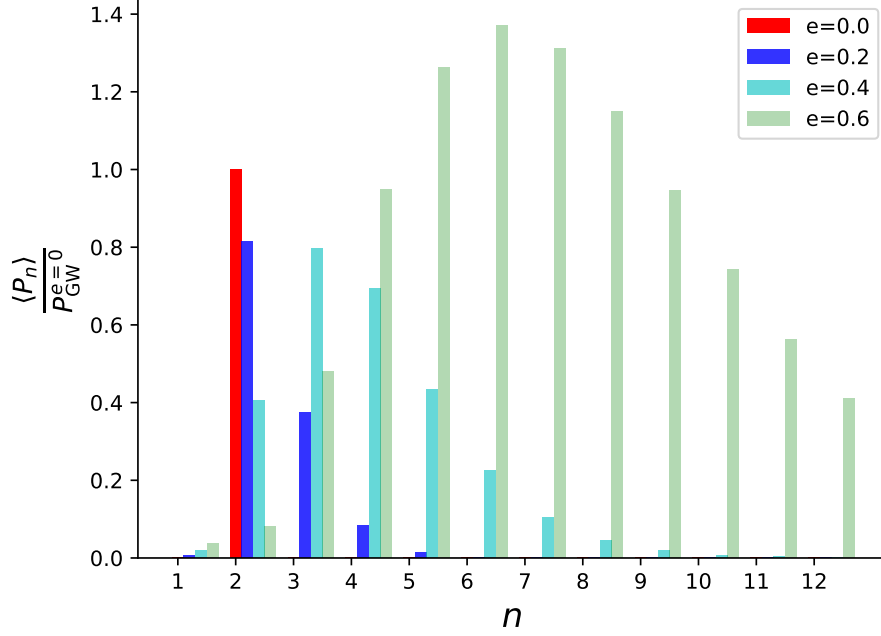


Figure 2.9: Plot of $\langle P_n \rangle / P_{\text{GW}}^{e=0}$ for different values of $e = 0$ (red), $e = 0.2$ (blue), $e = 0.4$ (cyan) $e = 0.6$ (green).

This combined with Eqs. [2.96] and Eq. [2.100] gives

$$\frac{dp}{dt} = -\frac{64}{5}\nu c \left(\frac{Gm}{c^2 p}\right)^3 (1-e^2)^{3/2} \left[1 + \frac{7}{8}e^2\right]. \quad [2.109]$$

The energy of the orbit is given in Eq. [2.73], from which

$$\dot{e} = \frac{1}{\nu G m^2} \frac{p}{e} \dot{E} - \frac{\dot{p}}{2pe} (1-e^2). \quad [2.110]$$

Then plugging in [2.99] and [2.109] gives

$$\frac{de}{dt} = -\frac{304}{15}\nu c \left(\frac{e}{p}\right) \left(\frac{Gm}{c^2 p}\right)^3 (1-e^2)^{3/2} \left[1 + \frac{121}{304}e^2\right]. \quad [2.111]$$

Notice that an initially circular orbit with $e = 0$ remains circular for all times. These coupled equations Eq. [2.109] and [2.111] can be solved together for $e(t)$ and $p(t)$, or alternatively combined to determine $p(e)$.

Observe that both $p(t)$ and $e(t)$ decrease with time. An elliptical orbit with initial eccentricity $e \neq 0$ will thus become more circular due to GW radiation. This is the reason why often it is a good approximation to consider circular orbits, particularly when studying the last moments before the merger of the binary system. (This is the case of the events observed by LVK.) The time-scale, τ_R , of the radiative decay of e and p can be estimated from say [2.111], which we rewrite as

$$\frac{de}{dt} \sim -\frac{e}{\tau_R}. \quad [2.112]$$

To lowest order in e this leads to

$$\tau_R = \frac{1}{\nu} \left(\frac{Gm}{c^2 p} \right)^{-5/2} \frac{T}{2\pi} \quad [2.113]$$

where T is the orbital period [2.74]. From Eq. [2.70], $\left(\frac{Gm}{c^2 p} \right) \sim |\vec{v}|^2/c^2 \ll 1$, and thus $\tau_R \sim (c/v)^{-5} T \gg T$.

The decrease of p and e also imply that T decreases with time. Indeed from Eqs. [2.74], [2.111] and [2.109]

$$\frac{dT}{dt} = -\frac{192}{5} \pi \left(\frac{GM}{c^3} \frac{2\pi}{T} \right)^{5/3} \left[\frac{1 + \frac{73}{24}e^2 + \frac{37}{96}e^4}{(1-e^2)^{7/2}} \right] \quad [2.114]$$

where \mathcal{M} is the chirp mass [1.6]. Thus the orbital frequency ω_0 increases, and GWs are emitted with increasing frequencies. Furthermore, from e.g. Eq. [2.89], the GW amplitude increases (since p decreases). In fact, to find the GW waveforms $h_{+, \times}$, the solutions of Eqs. [2.111] and [2.109] for $e(t)$ and $p(t)$ must be substituted into Eq. [2.68] namely

$$\frac{d\psi(t)}{dt} = \sqrt{\frac{Gm}{p^3(t)}} [1 + e(t) \cos(\psi(t))]^2 \quad [2.115]$$

from which one determines $\psi(t)$. The waveform $h_{+, \times}$ are then given by e.g. [2.87] and [2.88] when $\vec{N} = \vec{e}_z$. The plus polarisation is plotted in Fig. 2.10 for 4 different initial values of the eccentricity $e = 0, 0.3, 0.5$ and 0.7 .

The upper waveform in Fig. 2.10 is for circular orbits. The increasing amplitude and frequency of the GWs is clearly visible and will be quantified in the

discussion below. The waveform diverges when p reaches zero, though clearly this is beyond the regime of applicability of the quadrupole approximation which assumes $|\vec{v}|/c \ll 1$. Since $|\vec{v}| \sim 1/\sqrt{p}$ this is clearly violated as $p \rightarrow 0$. That is the reason why, in Section 1.1.4.2, we invoked the ISCO as a possible minimum distance, which then defined a merger frequency through Eq. [1.8].

The lower three curves shows h_+ for increasing initial eccentricity. The elliptical nature of the orbits is reflected in the waveform which, while periodic is no longer symmetric with maximum power emitted at the pericenter. Furthermore, as discussed above, a consequence of the Peter Mathews equation is that the emitted GW power increases with e . This is why the waveform diverges at earlier and earlier times as e increases. Finally, in figure 2.11 we plot the orbits of the system for $e = 0$ and $e = 0.3$. The decrease in orbital radius and eccentricity is clear from the figure.

2.4.4. Circular orbits: analytic expressions

It is straightforward to write down analytical solutions for circular orbits of radius $p(t)$. As discussed above, all GW waves are emitted with frequency $f(t)$ and angular frequency $\omega(t)$ which satisfy

$$\omega(t) = 2\pi f(t) = 2\omega_0 = 2\sqrt{\frac{Gm}{p^3(t)}} \quad [2.116]$$

from [2.74]. Using Eq. [2.109] with $e = 0$, the time dependence of ω can then be straightforwardly determined, giving

$$\dot{\omega} = \frac{12}{5} 2^{1/2} \left(\frac{G\mathcal{M}}{c^3}\right)^{5/3} \omega^{11/3} \quad [2.117]$$

or equivalently in terms of $f = \omega/2\pi$,

$$\dot{f} = \frac{96}{5} \pi^{8/3} \left(\frac{G\mathcal{M}}{c^3}\right)^{5/3} f^{11/3} \quad [2.118]$$

where \mathcal{M} is again the chirp mass Eq. [1.6]. Integration directly gives $f(t)$, namely

$$f(\tau) = \frac{1}{\pi} \left(\frac{5}{256\tau}\right)^{3/8} \left(\frac{G\mathcal{M}}{c^3}\right)^{-5/8} \quad [2.119]$$

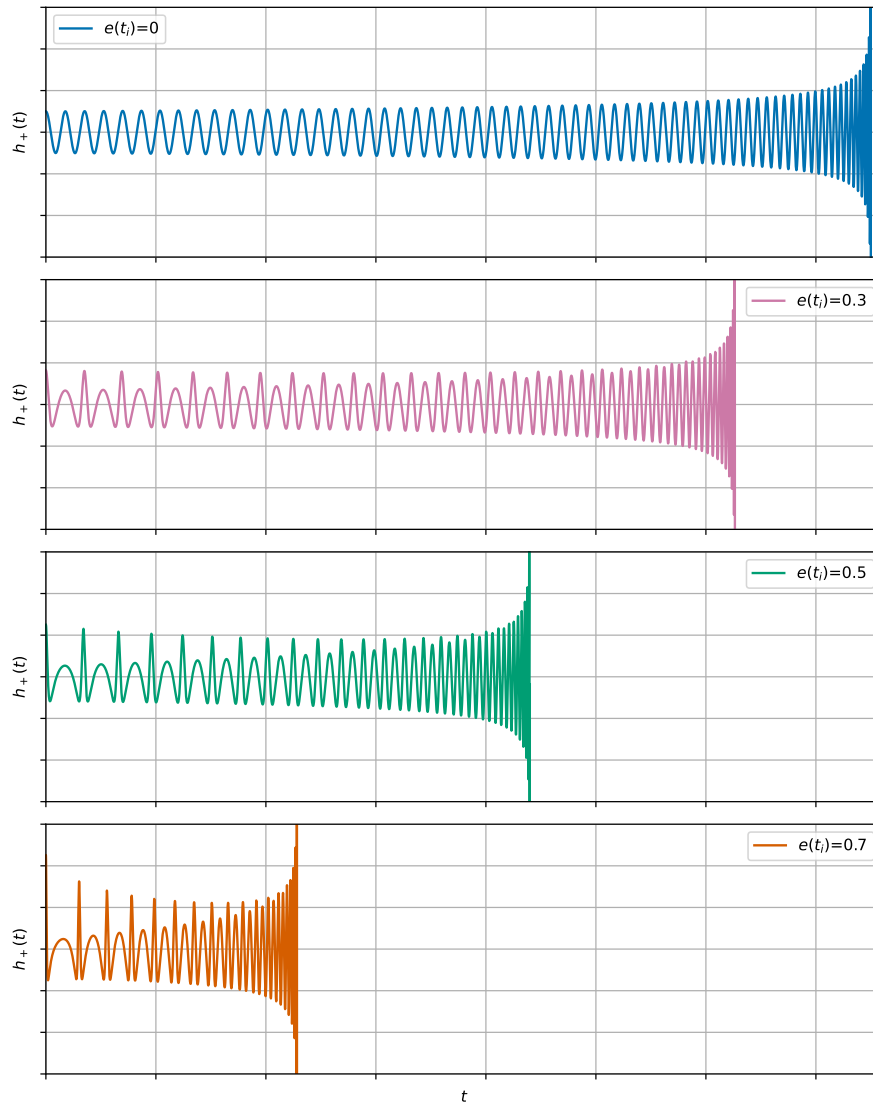


Figure 2.10: Four waveforms, in the lowest order PN expansion, with initial values of eccentricity given by $e = 0, 0.3, 0.5$ and 0.7 . Most GW power is emitted near the pericenter where the orbital velocity is the largest. Also since more GW radiation is emitted as e increases, the merger occurs earlier.

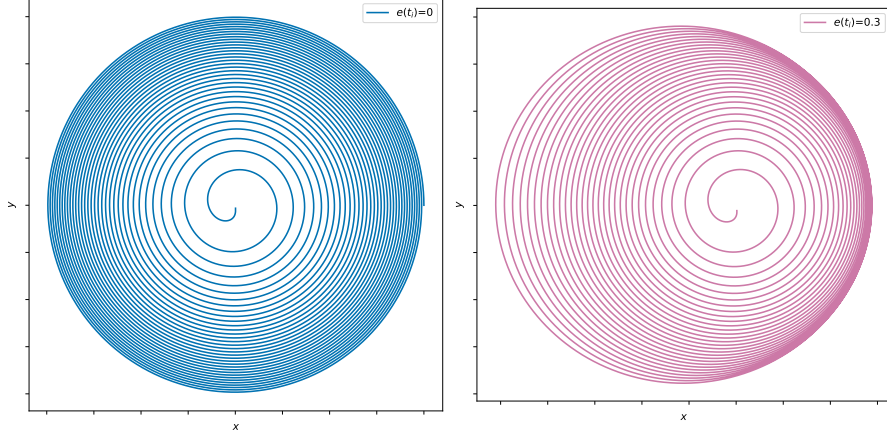


Figure 2.11: Corresponding to Fig. 2.10, the orbits $r(t)$ given by Eq. [2.65] for $e = 0$ and $e = 0.3$

where $\tau = t - t_c$ and as in section 1.1.4.1, t_c is the coalescence time where f formally diverges. (This corresponds to the time at which the waveform diverges in figure 2.10.) Thus for a binary inspiral on a circular orbit $f^{-8/3}$ is linear in time, with a slope which determines directly the chirp mass.

Now, from [2.87] with $e = 0$, the GW phase is $\Phi \equiv 2\psi$ which from [2.115] satisfies $d\Phi/dt = 2\omega(t)$. Thus

$$\Phi(t) = 2 \int_{t_i}^t dt' \omega(t'). \quad [2.120]$$

Combining these results and using Eq. [1.91], the plus and cross polarisations in some direction \vec{N} (described by θ and φ) are given by

$$h_+(t) = \frac{4}{R} \left(\frac{GM}{c^2} \right)^{5/3} \left(\frac{\pi f(t_R)}{c} \right)^{2/3} \cos[\Phi(t_R) + \phi] \left(\frac{1 + \cos^2 \theta}{2} \right) \quad [2.121]$$

$$h_\times(t) = \frac{4}{R} \left(\frac{GM}{c^2} \right)^{5/3} \left(\frac{\pi f(t_R)}{c} \right)^{2/3} \sin[\Phi(t_R) + \phi] \cos \theta. \quad [2.122]$$

The angle θ can be identified with the inclination of the source relative to the detector, see Fig. 1.1, while ϕ can be reabsorbed into a redefinition of time; indeed from [2.120] and [2.117] using that $d\tau = -dt$,

$$\Phi(\tau) = -2 \left(\frac{5GM}{c^3} \right)^{-5/8} \tau^{5/8} + \Phi_c \quad [2.123]$$

where Φ_c is the phase at $\tau = 0$ namely at coalescence. Thus to conclude

$$h_+(t) = \frac{1}{R} \left(\frac{GM}{c^2} \right)^{5/4} \left(\frac{5}{c\tau} \right)^{1/4} \left[\frac{1 + \cos^2 \iota}{2} \right] \cos \Phi(\tau) \quad [2.124]$$

$$h_\times(t) = \frac{1}{R} \left(\frac{5GM}{c^2} \right)^{5/4} \left(\frac{5}{c\tau} \right)^{1/4} \cos \iota \sin \Phi(\tau) \quad [2.125]$$

where $\theta = \iota$ is the inclination of the binary, see Fig. 1.1. This is the analytic expression of the curve plotted in blue in figure 2.10.

2.4.5. Hyperbolic orbits

While all GW detections to date are from *bound* elliptical/circular CBCs with $e < 1$, many other potential GW sources exist for instance non-spherical spinning NSs and asymmetric core collapse Supernovae. In this brief subsection we discuss another possible source, namely *unbound binary systems on hyperbolic orbits*. That is, we consider cases in which the eccentricity $e > 1$ see Eq. [2.73] and Fig. 2.12.

Hyperbolic orbits are interesting not only because unbound orbits are expected to exist in nature (and hence the waveform for such events is and will be searched for by GW detectors (Agazie *et al.* 2024 ; Gasparotto *et al.* 2023 ; Goncharov *et al.* 2024 ; Inchauspé *et al.* 2024)), but also because this simple system provides a first example of a *gravitational wave memory effect*. There are many different kinds of memory effects (see e.g. (Favata 2010)), the simplest of which is the linear memory effect which occurs already at the lowest order in the PN expansion and which is illustrated by hyperbolic orbits. Memory effects occur when there is a permanent change $\Delta h_{ab}^{\text{TT}}$ in the gravitational waveform, and thus leads to permanent displacement ΔL of the arms of GW detector for example, see Eq. [2.4].

2.4.5.1. Linear memory effect and low-frequency GWs

The two GW polarisations for hyperbolic orbits are shown in Fig. 2.8 for $\vec{N} = (0, 0, 1)$. The waveform is not periodic but rather burst-like, and h_\times has

a non-zero variation between $t = \pm\infty$: this is the linear memory effect. More generally, the variation of the metric perturbation between $t = \pm\infty$ is given by

$$\Delta h_{cd}^{\text{TT}} = \int_{-\infty}^{\infty} dt \dot{h}_{cd}^{\text{TT}}(t), \quad [2.126]$$

thus it follows from [2.45] that there will be a linear memory effect $\Delta h_{ij}^{\text{TT}} \neq 0$ when there is a *net change in the second time derivatives of quadrupole moments* of the system. This is precisely the case for hyperbolic orbits. Indeed, it is

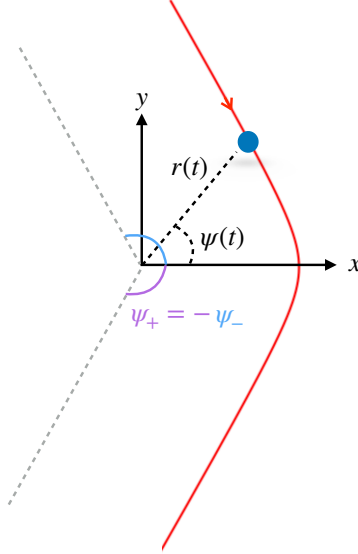


Figure 2.12: Sketch of a hyperbolic orbit in the CM, showing the angles $\psi_{\pm} = \pm \arccos(-1/e)$.

straightforward to show that

$$\begin{aligned} \Delta h_{cd}^{\text{TT}} &= h_{cd}^{\text{TT},+} - h_{cd}^{\text{TT},-} = \frac{2G}{c^4 R} P^{\text{TT}ab}(\vec{N})(\ddot{I}_{ab}^+ - \ddot{I}_{ab}^-) \\ &= -\frac{4G\nu}{c^4 R} v_{\infty}^2 \frac{\sqrt{e^2 - 1}}{e^2} P^{\text{TT}ab}(\vec{N})(\delta_{a,x}\delta_{b,y} + \delta_{b,x}\delta_{a,y}). \end{aligned} \quad [2.127]$$

where v_{∞} is given in Eq. [2.77].

The time-scale over which the GW signal varies in Fig 2.8 varies, namely the burst time-scale, is determined by the inverse of the characteristic frequency ω_c^{-1} given in Eq. [2.76]. Up to factors of eccentricity, this also determines the characteristic frequency scale of the emitted GWs on hyperbolic orbits. Indeed, contrary to the case of periodic elliptical orbits discussed in section 2.4.3.2, now GWs of all continuous frequencies are emitted, and one can determine the GW power as a function of frequency by now Fourier transforming the power emitted. Using the convention $\tilde{I}_{ab}(\omega) = \int dt I_{ab}(t) e^{-i\omega t}$, as well as the quadrupole approximation, the total energy emitted in GWs is

$$E_{\text{GW}} = \frac{G}{5c^5} \int_{-\infty}^{\infty} dt (\ddot{I}_{ab})^2 = \frac{G}{5\pi c^5} \int_0^{\infty} d\omega \omega^6 |I_{ab}(\omega)|^2 \equiv \int_0^{\infty} d\omega \mathcal{P}_{\text{GW}}(\omega).$$

Thus the emitted power in GWs is thus

$$\mathcal{P}_{\text{GW}}(\omega) = \frac{G}{5\pi c^5} [\omega^3 \tilde{I}_{ab}(\omega)] [\omega^3 \tilde{I}_{ab}^*(\omega)]. \quad [2.128]$$

Direct calculation analogous to that of section 2.4.3.1 (see e.g. (Brax and Steer 2024)) shows that $\mathcal{P}_{\text{GW}}(\omega)$ is peaked at a value fixed by ω_c but which increases with e , see figure 2.13. Notice that $\mathcal{P}_{\text{GW}}(0) \neq 0$. This is due to the linear memory effect: indeed Eq. [2.126], written in Fourier space reads

$$\Delta h_{cd}^{\text{TT}} = -i \frac{2G}{c^4 R} P^{\text{TT}ab}(\vec{N}) [\omega^3 \tilde{I}_{ab}(\omega)]|_{\omega=0}, \quad [2.129]$$

thus a non-vanishing linear memory effect implies $\mathcal{P}_{\text{GW}}(0) \neq 0$.

2.4.5.2. Capture due to GW emission

One can estimate the energy emitted in GWs between $\psi_- < \psi < 0$ by calculating

$$\Delta E_{\text{GW}} = \int_{\psi_-}^0 d\psi \frac{1}{\dot{\psi}} P_{\text{GW}}(\psi) \quad [2.130]$$

where $P_{\text{GW}}(\psi)$ is given in Eq. [2.92]. Let us consider an orbit which is only slightly unbound, thus $e = 1 + \epsilon$ with $0 < \epsilon \ll 1$ so that the orbital energy is $E \simeq \nu G m^2 \epsilon / p$, see Eq. [2.73]. Then it is straightforward to determine ΔE_{GW} to lowest order in ϵ , leading to

$$\Delta E_{\text{GW}} = \frac{85}{3} m c^2 \nu^2 \left(\frac{Gm}{c^2 p} \right)^{7/2} \pi + \mathcal{O}(1). \quad [2.131]$$

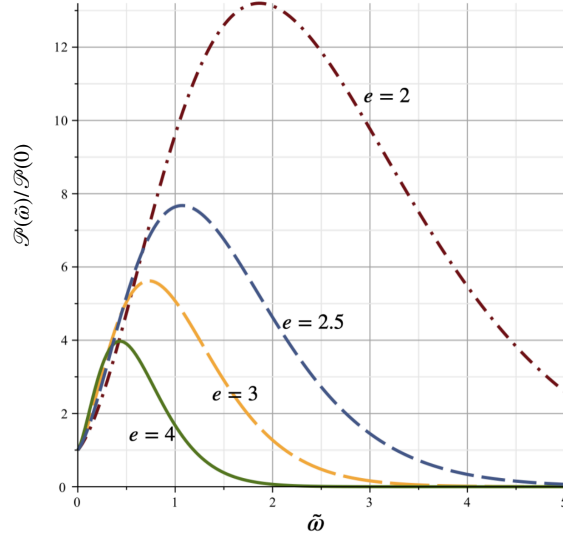


Figure 2.13: The energy spectrum $\mathcal{P}_{\text{GW}}(\tilde{\omega})/\mathcal{P}_{\text{GW}}(0)$ where $\tilde{\omega} = \omega/\omega_c$ for different eccentricities. Figure from (Brax and Steer 2024).

Note that here we assumed p constant, that is we have neglected the back-reaction of the emitted GR on p : this is a reasonable approximation for this individual burst process since p changes on a time-scale $\sim (c/v)^{-5}\omega_c^{-1}$ as discussed previously. The orbital energy $E \sim \nu Gm^2\epsilon/p$ will thus be reduced by ΔE_{GW} , and if

$$E - \Delta E_{\text{GW}} < 0 \quad [2.132]$$

then the GW energy loss will convert the hyperbolic orbit into a bound orbit before the pericenter. This can be rewritten as the condition

$$\epsilon < \frac{85\nu}{3} \left(\frac{Gm}{c^2 p} \right)^{5/2} \pi. \quad [2.133]$$

Instead of parametrising the orbit in terms of (p, ϵ) , for such scattering trajectories it is more convenient to work with (b, v_∞) where b is the impact parameter and v_∞ is the orbital velocity at infinite separation. From Eq. [2.77], $v_\infty^2 \simeq 2(Gm/p)\epsilon$ and substituting ϵ from Eq. [2.133] gives

$$\left(\frac{Gm}{c^2 p} \right)^{7/2} > \frac{3}{170\pi\nu} \left(\frac{v_\infty}{c} \right)^2. \quad [2.134]$$

Furthermore, basic trigonometry gives

$$b = \frac{p}{\sin \psi_-} = \frac{pe}{\sqrt{e^2 - 1}} \simeq \frac{p}{\sqrt{2\epsilon}} = \frac{\sqrt{Gmp}}{v_\infty}. \quad [2.135]$$

Saturating the bound in [2.134] identifies the impact parameter b_{capture} for which capture occurs. The corresponding capture cross-section $\sigma_{\text{GW}} := \pi b_{\text{capture}}^2$ is thus given by

$$\sigma_{\text{GW}} = \pi \left(\frac{170\pi\nu}{3} \right)^{2/7} \left(\frac{Gm}{c^2} \right)^2 \left(\frac{c}{v_\infty} \right)^{18/7}. \quad [2.136]$$

Such a process could play an important role for instance in dense star clusters and galactic nuclei, see e.g. (Capozziello *et al.* 2008 ; O’Leary *et al.* 2009 ; Hoang *et al.* 2020).

2.5. GWs in curved space-time, cosmology

In the previous sections we discussed GWs in Minkowski space; our aim is now to generalise the results presented there to a cosmological space-time. There is now a further scale of interest other than the characteristic size d of the source and the GW wavelength λ_{GW} , namely the *cosmological horizon*. The results of the previous sections are valid in the so-called the *local wavezone* of the source, namely at distances scales R which are large compared to the GW wavelength but *small* compared to the cosmological horizon, $d \ll \lambda_{\text{GW}} \ll R \ll \text{horizon}$. We now aim to extend them to cosmological scales: we will see that the expansion of the universe dampen the GW amplitude, and redshift frequencies and masses.

2.5.1. General background metric

2.5.1.1. Linearised equations

The linearized equations around an arbitrary background [1.34] are given explicitly in Appendix 1.4. We can simplify them again using the de Donder gauge [1.74], generalised to curved space-time as¹¹

$$\bar{\nabla}^\mu \bar{h}_{\mu\nu} = 0, \quad \bar{h}_{\mu\nu} := h_{\mu\nu} - \frac{1}{2} \bar{g}_{\mu\nu} h. \quad [2.137]$$

11. We are using a bar to indicate both the background metric, and the trace-reversed perturbation. We believe that no confusion should arise, because of the different places where these quantities enter.

In this gauge, the equations of motion become in empty space (see Eq. [1.139])

$$\square \bar{h}_{\alpha\beta} + 2\bar{R}^{\mu}{}_{\alpha\nu\beta} \bar{h}^{\nu}{}_{\mu} + S_{\mu\alpha\nu\beta} \bar{h}^{\mu\nu} = 0 \quad [2.138]$$

where, see Eq. [1.140],

$$S_{\mu\alpha\nu\beta} = 2\bar{G}_{\mu(\alpha} g_{\beta)\nu} - \bar{R}_{\mu\nu} g_{\alpha\beta}. \quad [2.139]$$

Here $\bar{R}_{\mu\alpha\nu\beta}$ is the Riemann curvature tensor of the background space-time, and $\bar{R}_{\mu\nu}$ the Ricci-tensor. The two last terms depend on the ratio of λ_{GW} relative to the scale of variation of the background metric. In the following we will assume that they are negligible. (For a homogeneous and isotropic FRLW metric¹², considered below, the scale of variation of the background is the cosmological horizon, which is much greater than λ_{GW} .) Thus Eq. 2.138 reduces to

$$\bar{g}^{\mu\nu} \bar{\nabla}_{\mu} \bar{\nabla}_{\nu} \bar{h}_{\alpha\beta} \simeq 0. \quad [2.140]$$

2.5.1.2. WKB approximation

For a general space-time, the solution of Eq. [2.140] can be obtained in the WKB approximation. The underlying physical assumption is that the amplitude of the wave is slowly varying with respect to the frequency of the wave, and hence we write

$$\bar{h}_{\mu\nu}(x) = \sum_p \Re \left[A_p(x) \epsilon_{\mu\nu}^p(x) e^{iS(x)/\delta} \right] \quad [2.141]$$

where the sum is over polarisations p with polarisation tensor $\epsilon_{\mu\nu}$ satisfying $\epsilon_{\mu\nu} \epsilon^{\mu\nu} = 1$ (recall that to this leading order in h , indices are raised and lowered with the background metric) and A is the corresponding amplitude. The parameter $\delta \rightarrow 0$, and we define

$$k^{\mu} = \frac{\partial_{\mu} S}{\delta}. \quad [2.142]$$

Now substituting [2.141] the de Donder condition Eq. 2.137 becomes (dropping the p sum for simplicity)

$$\bar{\nabla}^{\mu} \bar{h}_{\mu\nu} = \left[\bar{\nabla}^{\mu} (A \epsilon_{\mu\nu}) + i A \epsilon_{\mu\nu} \frac{\partial_{\mu} S}{\delta} \right] e^{iS(x)/\delta} = 0, \quad [2.143]$$

12. In a perturbed FRLW metric, there could be local bumps in the curvature of scale similar to λ_{GW} : we do not consider this case here.

which to leading order in δ implies

$$k^\mu \epsilon_{\mu\nu} = 0 \quad [2.144]$$

and hence that $\epsilon_{\mu\nu}$ is the transverse polarisation tensor. Substitution into the equation of motion Eq. [2.140] leads to terms in δ^{-2} , δ^{-1} which are, respectively

$$\bar{g}^{\mu\nu} k_\nu k_\mu = 0, \quad [2.145]$$

$$2\bar{\nabla}_\mu (A\epsilon_{\alpha\beta})k^\mu + (A\epsilon_{\alpha\beta})\bar{\nabla}_\mu k^\mu = 0. \quad [2.146]$$

The first equation, the Eikonal equation (geometric optics limit), implies that GWs are massless with dispersion relation $\omega^2 = \vec{k}^2$ and propagate on null geodesics. Contracting the second equation [2.146] with $\epsilon^{\alpha\beta}$, and using that $\epsilon_{\mu\nu}\epsilon^{\mu\nu} = 1$ so that $(\bar{\nabla}^\alpha \epsilon_{\mu\nu})\epsilon^{\mu\nu} = 0$, leads to

$$2(\bar{\nabla}_\mu A)k^\mu + A\bar{\nabla}_\mu k^\mu = 0 \quad \Rightarrow \quad \bar{\nabla}_\mu (A^2 k^\mu) = 0. \quad [2.147]$$

This gives the decay of the GW amplitude A along the null geodesics. Finally, substituted back Eq. [2.147] into Eq. [2.146] gives

$$k^\mu (\bar{\nabla}_\mu \epsilon_{\alpha\beta}) = 0 \quad [2.148]$$

which implies that the polarization tensor $\epsilon_{\alpha\beta}$ of the GW is parallel propagated along the null geodesics.

To summarise, in the Lorenz gauge, the solution of

$$\bar{g}^{\mu\nu} \bar{\nabla}_\mu \bar{\nabla}_\nu \bar{h}_{\alpha\beta} \simeq 0 \quad [2.149]$$

in the WBK approximation is $\bar{h}_{\mu\nu}(x) = \Re [A(x)\epsilon_{\mu\nu}(x)e^{ik_\mu x^\mu}]$ with

$$\bar{g}^{\mu\nu} k_\nu k_\mu = 0 \quad [2.150]$$

$$k^\mu \epsilon_{\mu\nu} = 0 \quad [2.151]$$

$$\bar{\nabla}_\mu (A^2 k^\mu) = 0 \quad [2.152]$$

$$k^\mu (\bar{\nabla}_\mu \epsilon_{\alpha\beta}) = 0 \quad [2.153]$$

We now consider these equations in a FRLW metric.

2.5.2. FRLW metric: background

The flat Friedmann-Robertson-Lemaitre-Walker (FRLW) metric is

$$d\bar{s}^2 = -dt^2 + a^2(t)d\bar{x}^2 = -dt^2 + a^2(t)(dr^2 + r^2d\Omega^2) \quad [2.154]$$

where \bar{x} are comoving coordinates and $a(t)$ is the scale factor (normalised such that today, at $t = t_0$, $a(t_0) \equiv a_0 = 1$). For a perfect fluid source, Einsteins equations Eq. [1.16] reduce to the Friedmann equations

$$H^2 = \frac{8\pi G}{3}\rho + \frac{\Lambda}{3} \quad [2.155]$$

$$\frac{\ddot{a}}{a} = -\frac{8\pi G}{6}(\rho + 3P) + \frac{\Lambda}{3} \quad [2.156]$$

where ρ and P are respectively the energy density and pressure of the perfect fluid, and $H = \frac{\dot{a}}{a}$ is the Hubble parameter, whose value today is the Hubble constant H_0 . These two equations imply the conservation equation $\dot{\rho} + 3H(\rho + P) = 0 = \nabla_\nu T^{\mu\nu}$. In terms of conformal time η defined by $d\eta = dt/a(t)$, the metric in Eq. [2.154] is conformally related to the Minkowski metric

$$d\bar{s}^2 \equiv \bar{g}_{\mu\nu}dx^\mu dx^\nu = a^2(\eta)[-d\eta^2 + dr^2 + r^2d\Omega^2]. \quad [2.157]$$

Consider now a source (of photons or GWs) at fixed radial position $r = 0$, and an observer at r_o . On a (η, r) space-time diagram null radial geodesics propagate at 45 degrees. If two null geodesics are emitted at a conformal time interval $\delta\eta_s$ by the source, then they arrive at the observer with the same conformal time interval $\delta\eta_o = \delta\eta_s$. This implies the standard time-dilation relation

$$dt_o = \frac{a(t_o)}{a(t_s)}dt_s \equiv (1+z)\bar{dt}_s \quad [2.158]$$

where z is the redshift of the source (the observer is at $t_o = t_0$), and equivalently that the emitted (or ‘source’) frequency f_s is related to the observed frequency f_o by

$$f_o = \frac{f_s}{1+z}. \quad [2.159]$$

The radial comoving distance R to an event with redshift z is given by solving $ds^2 = 0$, thus $dr = dt/a(t)$, leading to

$$R = \int dr = \int \frac{dt}{a(t)} = \int \frac{1}{a} \frac{dt}{da} da dz = \int_0^z dz \frac{1}{H(z)} \quad [2.160]$$

where $H(z) = H_0 E(z)$ is the Hubble parameter expressed in terms of redshift, and from the Friedmann equation

$$E(z) = \sqrt{\Omega_m(1+z)^3 + \Omega_r(1+z)^4 + \Omega_\Lambda} \quad [2.161]$$

where $\Omega_{r,m} = \frac{8\pi G\rho_{r,m}}{3H_0^2}$, $\Omega_\Lambda = \frac{\Lambda}{3H_0^2}$ and $\Omega_r + \Omega_m + \Omega_\Lambda = 1$.

A crucial quantity is the luminosity distance $d_L(z)$. This relates the EM luminosity of the source and the luminosity measured by the observer. In the flat FRWL metric [2.154] it is given by

$$d_L(z) = a(t_o)(1+z)R = (1+z) \int_0^z dz \frac{1}{H(z)} \quad [2.162]$$

As we will see, this same distance scale determines the GW amplitude in an expanding universe.

2.5.3. FRLW metric: gravitational waveforms

Consider a GW propagating radially outwards from the source at $r = 0$ and redshift z_s with $k_\mu = \omega(1, -1, 0, 0)$. From Eq. [2.147] it is possible to determine how the GW amplitude decreases along the null GW geodesic. In a FRLW metric (in conformal time) Eq. [2.147] becomes

$$\partial_\nu(\sqrt{-\bar{g}}A^2k^\nu) = 0 = \partial_\nu(a(\eta)^2A^2r^2k^\nu). \quad [2.163]$$

Thus $A(\eta, r)a(\eta)r$ remains conserved during the propagation, and

$$A(\eta, r) = \frac{\text{const}}{a(\eta)r} \Big|_{\eta-r=\text{const}} \quad [2.164]$$

The constant is fixed by the known amplitude of the wave in the wave-zone approximation, close to the source, where the Minkowski results are valid. Then the remainder of the solution $\bar{h}_{\mu\nu}$ is obtained by parallel transporting this solution from the source to the observer. We now carry out these steps.

Before doing so we note that in a flat FRLW universe and focusing on the *spatial* TT components only, then in fact [2.138] reduces to identically to

$$\bar{g}_{\mu\nu}\bar{\nabla}^\mu\bar{\nabla}^\nu\bar{h}_{ij}^{\text{TT}} = 0 = h_{ij}^{\text{TT}''} + 2\mathcal{H}h_{ij}^{\text{TT}'} + \partial_k\partial^k h_{ij}^{\text{TT}} \quad [2.165]$$

since the spatial components of the Riemann and Ricci tensors vanish identically. From here the scaling of the amplitude of GWs as $1/a(\eta)$ is also immediate.

We now consider a compact binary system on circular orbits, as discussed in section 2.4.4 in Minkowski space. In the wavezone approximation and at a physical distance $R = a(t_s)r$ from the source as measured by time t_s of the source clock, the plus and cross polarisations of the GW are given in [2.121] and [2.122]. Focusing on the cross polarisation,

$$h_{\times}(t_s, \iota) = \frac{4}{R} \left(\frac{GM}{c^2} \right)^{5/3} \left(\frac{\pi f_s(t_s^{\text{ret}})}{c} \right)^{2/3} \cos \iota \sin(2\Phi_s(t_s^{\text{ret}})) \quad [2.166]$$

where $t_s^{\text{ret}} = t_s - t_c$ is the time to coalescence at t_c and \mathcal{M} is the chirp mass [1.6]. The time dependence of the frequency is given in Eq. [2.118] namely

$$\frac{df_s}{dt_s} = \frac{96}{5} \pi^{8/3} \left(\frac{GM}{c^3} \right)^{5/3} f_s^{11/3} \quad [2.167]$$

leading to

$$f_s(t_s^{\text{ret}}) = \frac{1}{\pi} \left(\frac{5}{256 t_s^{\text{ret}}} \right)^{3/8} \left(\frac{GM}{c^3} \right)^{-5/8}, \quad [2.168]$$

so that the phase dependence is

$$\Phi_s(t_s) = \Phi_c + 2\pi \int_{t_c}^{t_s} dt'_s f_s(t'_s) = -2 \left(\frac{t_s^{\text{ret}} c^3}{5GM} \right)^{5/8} + \Phi_c. \quad [2.169]$$

We now parallel transport this solution [2.166] along a null geodesic to the observer. Along the geodesic the GW phase remains constant because the time dilation effects cancel the redshifting of the frequency. Thus at the observer whose clock measures $dt = dt_s(1+z)$, the observed GW frequency $f = f_s/(1+z)$ leading to $\Phi(t) = \Phi_s(t_s)$. However, at the observer, the GW amplitude is changed. From Eq. [2.164], and using [2.166]

$$h_{\times}(t, \iota) = \frac{4}{a(t)R} \left(\frac{GM}{c^2} \right)^{5/3} \left[\frac{\pi}{c} f(t^{\text{ret}})(1+z) \right]^{2/3} \cos \iota \sin(2\Phi(t^{\text{ret}})) \quad [2.170]$$

where we have included the redshifting of frequency. Let us now define the *redshifted chirp mass*

$$\mathcal{M}_z = (1+z)\mathcal{M} \quad [2.171]$$

Then [2.170] becomes

$$\begin{aligned} h_{\times}(t, \iota) &= \frac{4}{a(t)R(1+z)} \left(\frac{G\mathcal{M}_z}{c^2} \right)^{5/3} \left(\frac{\pi f(t^{\text{ret}})}{c} \right)^{2/3} \cos \iota \sin(2\Phi(t^{\text{ret}})) \\ &= \frac{4}{d_L(z)} \left(\frac{G\mathcal{M}_z}{c^2} \right)^{5/3} \left(\frac{\pi f(t^{\text{ret}})}{c} \right)^{2/3} \cos \iota \sin(2\Phi(t_o^{\text{ret}})) \end{aligned}$$

where in the second line we have used Eq. [2.162] defining the luminosity distance to the source (today $a(t_o) = 1$). The dependence of the observed frequency on time t is obtained by $f_s = (1+z)f$ into Eq. [2.167]:

$$(1+z) \frac{d[f(1+z)]}{dt} = \frac{96}{5} \pi^{8/3} \left(\frac{G\mathcal{M}}{c^3} \right)^{5/3} f^{11/3} (1+z)^{11/3}. \quad [2.172]$$

Assuming that changes in z are negligible during the observation time, then z can be taken as constant¹³ leading to

$$\frac{df}{dt} = \frac{96}{5} \pi^{8/3} \left(\frac{G\mathcal{M}_z}{c^3} \right)^{5/3} f^{11/3}, \quad [2.173]$$

namely the GW phase depends on the *redshifted chirp mass*,

$$\Phi(t^{\text{ret}}) = -2 \left(\frac{t^{\text{ret}} c^3}{5G\mathcal{M}_z} \right)^{5/8} + \Phi_c. \quad [2.174]$$

To summarize, the GW frequency depends on the redshifted chirp mass \mathcal{M}_z which is therefore determined by measurements of the phase of an inspiral signal. The GW amplitude depends on both \mathcal{M}_z and $d_L(z)$. Given that the former is determined from the phase, measurements of the amplitude of the signal determine $d_L(z)$. Generally speaking therefore, GW observations from

13. See (Bonvin *et al.* 2017) for a discussion of where this assumption may lead to biases

individual CBC events determine the luminosity distance $d_L(z)$ and the so-called ‘redshifted’ masses,

$$m_{1,2}^{\text{detected}} = (1+z)m_{1,2} \quad [2.175]$$

which are related to the ‘source’ masses $m_{1,2}$ by the same factor of $1+z$ as in Eq. [2.171].¹⁴

Notice that while redshift does change the waveform it occurs in such a way that can be exactly compensated by a shift of the masses from their ‘source’ to ‘detected’ values and by replacing the comoving distance with the luminosity distance. In other words, *it is not possible to determine the redshift z of the source from GW observations*: there is a perfect degeneracy between source masses, redshift, as well as spins. This is true to all orders in the PN expansion and is a consequence of the fact that GR is scale-free. (For NS binaries or NS-BH binaries, due to the non-zero NS radius R_{NS} and tidal effects this degeneracy is broken see e.g. (Del Pozzo *et al.* 2017 ; Messenger and Read 2012) and references within.)

If a cosmological model is assumed like Λ CDM, with given values of H_0 , Ω_m etc (say from the Planck observations), then of course from the measurement of the luminosity distance of an event, it is possible to determine z using Eq. [2.162]. Then, from the detected masses $m_{1,2}^{\text{detected}}$ one can determine the value of the source masses $m_{1,2}$ via Eq. [2.175]. This for example was done in (Abbott *et al.* 2016) which gives the source-frame values of the two black hole masses. However, in fact the values of the cosmological parameters H_0 etc are not precisely known, and a source of tension in cosmology today, see e.g. (Di Valentino *et al.* 2021). For these reasons, it can be interesting to use GW observations in a different way, namely as a new observable with which to measure cosmological parameters.

2.5.4. Measuring cosmological parameters with GWs

By definition, see [2.162], the luminosity distance $d_L(z)$ is a function of cosmological parameters such as H_0 , Ω_m . At small redshifts $z \ll 1$, the domain of the current O3 measurements of the LVK collaboration (Abbott *et al.* 2023), Eq. [2.162] reduces to

$$cd_L \sim \frac{z}{H_0} \quad [2.176]$$

14. To determine each mass individually, rather than in the combination of the chirp mass, requires the waveform beyond the lowest order quadrupolar form discussed here

meaning that only H_0 enters. Clearly, in order to measure H_0 not only is d_L required (and obtained from GW observations, as mentioned above), but the redshift z of the source. However, this cannot be determined from GW observations: extra non-gravitational information is necessary to determine z . Such information could be for example electro-magnetic.

The most straightforward way to determine z is to uniquely identify the “host galaxy” of the GW signal, namely the galaxy in which GW event occurred. This was possible for event GW170817 corresponding to the merger of 2 NS, which occurred on August 17th 2017. Indeed, 1.7s following the merger of the GWs observed by the two LIGOs and Virgo, EM observers around the globe observed a subsequent gamma-ray burst as well as multiple EM signals in different frequency bands. This EM data located the host galaxy down to NGC 4993, a galaxy in the Hydra constellation which is receding from us with a velocity $cz = 3327 \pm 72$ km/s, due to the expansion of the universe. Combining this with the distance $d_L = 43.8_{-6.9}^{+2.9}$ Mpc inferred from the GW signal led to an estimated value for $H_0 = 70_{-8}^{+12}$ km/s/Mpc (Abbott *et al.* 2017). This result, using one GW event only, is consistent with other measurements but of course less accurate because of its larger error bars. Its interest is that it shows that the idea works. The errors would be reduced (with a $1/\sqrt{N}$ scaling) if N other measurements of this kind existed, but unfortunately, GW170817 was an extremely rare event as since then no further GW events with associated EM counterparts (known as *standard sirens*) have been detected,

However, LVK has detected GWs from hundreds of BBHs and a few NS-BH, for each of which there is a measured d_L and $m_{1,2}^{\text{detected}}$ — but no EM counterpart. Even for these *dark sirens*, it is possible to obtain redshift information, and therefore measure H_0 . Today, two pieces of information are used together to get a statistical redshift for GW events: (i) galaxy catalogues and (ii) astrophysical modelling of the formation channels of BBHs. We refer the reader to (Mastrogiovanni *et al.* 2023) for a review of these methods and results.

2.6. Acknowledgements

We are grateful to Abhay Ashtekar, Eanna Flanagan, Cédric Deffayet, Alejandro Perez, Eric Poisson, Carlo Rovelli, Robert Wald for discussions on the topics of this review, as well as multiple Master 2 and doctoral students whom we have had the pleasure to teach over the years. We also thank ChatGPT for technical support (not for the calculations though!). This work was supported in part by Perimeter Institute for Theoretical Physics. Research at Perimeter Institute is supported by the Government of Canada through the Department of Innovation, Science and Economic Development and by the Province of Ontario through the Ministry of Research, Innovation and Science. This work was also supported in part by CERN.

2.7. Appendix: Landau-Lifshitz approach

The Landau-Lifshitz formulation of Einstein's equations is a convenient approach to perturbative theory around Minkowski, and it is widely used by the community working on the PN and PM expansions. We provide here a brief description of the approach from the perspective of the main text, and refer the reader to (Blanchet 2006 ; Poisson and Will 2014) for more details. In the Landau-Lifshitz approach one uses a density-weighted inverse metric as fundamental variable,

$$\mathfrak{g}^{\mu\nu} := \sqrt{-g}g^{\mu\nu} = \bar{g}^{\mu\nu} - \bar{h}^{\mu\nu} + O(h^2). \quad [2.177]$$

The interest in doing so is that the quantity

$$H^{\alpha\mu\beta\nu} := \mathfrak{g}^{\alpha\beta}\mathfrak{g}^{\mu\nu} - \mathfrak{g}^{\alpha\nu}\mathfrak{g}^{\beta\mu} \quad [2.178]$$

is related to the Einstein tensor via ordinary derivatives. More precisely,

$$\partial_\mu\partial_\nu H^{\alpha\mu\beta\nu} = 2(-g)(G^{\alpha\beta} + \frac{8\pi G}{c^4}t_{\text{LL}}^{\alpha\beta}) \doteq \frac{16\pi G}{c^4}(-g)(T^{\alpha\beta} + t_{\text{LL}}^{\alpha\beta}), \quad [2.179]$$

where $t_{\text{LL}}^{\alpha\beta}$ is a density-weight two pseudo-tensor, given explicitly by some lengthy expression in terms of first derivatives of the metric. Crucially, it is conserved on-shell $\partial_\alpha(-gt_{\text{LL}}^{\alpha\beta}) \doteq 0$. The dimension-full numerical factor in front of it is included in its definition for convenience when going on-shell in the last equality above.

This arrangement of Einstein's equations manifestly breaks covariance.¹⁵ Not only we have partial derivatives as opposed to covariant derivatives, but also tensor densities, aka pseudo-tensors, appearing. Its usefulness is limited to situations in which there are regions of spacetimes that are approximately flat, and where one can choose a Cartesian coordinate system, so that partial derivatives can be interpreted. This is precisely the case when studying a perturbative approximation around Minkowski. Within that context, the reformulation has two useful advantages.

The first is that it provides a prescription for a gravitational energy-momentum pseudo-tensor valid to all orders, given by $t_{\text{LL}}^{\alpha\beta}$. By analogy

15. It is like rearranging the covariant geodesic equation [2.1] as in [2.2], where neither side of the equation is covariant by itself.

with the matter counterpart, one has a prescription to further split this quantity into contributions to energy, momentum and angular momentum. All these expressions are gauge-dependent; in particular, we have the usual problem that the pseudo-tensor can be made to vanish at any given point, using a local inertial frame. But the logic in this approach is that we assume to have a preferred coordinate system, the Cartesian ones of the fiducial flat metric, and that is the gauge we stick to. Furthermore, since the left-hand side is a total derivative, the total energy, momentum and angular momentum can be expressed as surface integrals. This provides a prescription for these quantities that can be evaluated in a region far from the sources, where one can safely assume that spacetime is approximately flat and use Cartesian coordinates, and computed to all order in perturbation theory.

The second advantage of the formulation is that one can change variables to $\hat{h}^{\mu\nu} := \eta^{\mu\nu} - \mathbf{g}^{\mu\nu}$, where $\eta^{\mu\nu}$ is a fiducial background metric for which the coordinates are Cartesian, and then [2.179] are equivalent to

$$\square h^{\mu\nu} \hat{=} -\frac{16\pi G}{c^4} \tau^{\mu\nu}, \quad \tau^{\mu\nu} := (-g)(T^{\mu\nu} + t_{\text{LL}}^{\mu\nu} + t_{\text{H}}^{\mu\nu} + t_{\text{NH}}^{\mu\nu}), \quad [2.180]$$

where $t_{\text{H}}^{\mu\nu}$ satisfies $\partial_{\mu}(-gt_{\text{H}}^{\mu\nu}) \equiv 0$, and $t_{\text{NH}}^{\mu\nu}$ does not but contains only terms that vanish in harmonic gauge. It follows that in the harmonic gauge,

$$\partial_{\mu} \tau^{\mu\nu} \hat{=} 0. \quad [2.181]$$

By means of introducing a fiducial flat background and a fixed choice of Cartesian coordinates on it, one can rewrite the exact Einstein's equations in the form of a fiducial flat spacetime wave equation with a (very) complicated source. This set-up offers itself to a practical iteration scheme for the perturbation theory. The idea is to solve the 'relaxed field equations' [2.180] alone, in harmonic gauge, and afterwards impose the gauge consistency condition [2.181]. What makes this particularly practical is that [2.181] can be imposed on the matter dynamics. See (Blanchet 2006 ; Poisson and Will 2014) for further details.

2.8. Bibliography

- Abbott, B. P. *et al.* (2016), Observation of Gravitational Waves from a Binary Black Hole Merger, *Phys. Rev. Lett.*, 116(6), 061102.
- Abbott, B. P. *et al.* (2017), A gravitational-wave standard siren measurement of the Hubble constant, *Nature*, 551(7678), 85–88.
- Abbott, R. *et al.* (2023), Constraints on the Cosmic Expansion History from GWTC-3, *Astrophys. J.*, 949(2), 76.

- Agazie, G. *et al.* (2024), The NANOGrav 12.5 yr Data Set: Search for Gravitational Wave Memory, *Astrophys. J.*, 963(1), 61.
- Andersson, N. (2019), *Gravitational-Wave Astronomy*, Oxford Graduate Texts, Oxford University Press.
- Blanchet, L. (2006), Gravitational Radiation from Post-Newtonian Sources and Inspiralling Compact Binaries, *Living Rev. Rel.*, 9(1), 1–114.
- Bonvin, C., Caprini, C., Sturani, R., Tamanini, N. (2017), Effect of matter structure on the gravitational waveform, *Phys. Rev. D*, 95(4), 044029.
- Brax, P., Steer, D. A. (2024), Scalar kicks and memory, , .
- Burnett, G. A. (1989), The high frequency limit in general relativity, *Journal of Mathematical Physics*, 30(1), 90–96.
URL: <https://doi.org/10.1063/1.528594>
- Capozziello, S., De Laurentis, M., De Paolis, F., Ingrosso, G., Nucita, A. (2008), Gravitational waves from hyperbolic encounters, *Mod. Phys. Lett. A*, 23, 99–107.
- Cutler, C. *et al.* (1993), The Last three minutes: issues in gravitational wave measurements of coalescing compact binaries, *Phys. Rev. Lett.*, 70, 2984–2987.
- Damour, T., Deruelle, N. (1985), General relativistic celestial mechanics of binary systems. i. the post-newtonian motion, *Annales de l'I.H.P. Physique théorique*, 43(1), 107–132.
URL: <http://eudml.org/doc/76291>
- Del Pozzo, W., Li, T. G. F., Messenger, C. (2017), Cosmological inference using only gravitational wave observations of binary neutron stars, *Phys. Rev. D*, 95(4), 043502.
- DeWitt, B. S. (2011), *1971's Bryce DeWitt's Lectures on Gravitation*, vol. 826 of *Lecture Notes in Physics*, Springer, Berlin, Heidelberg.
URL: <https://doi.org/10.1007/978-3-540-36911-0>
- Di Valentino, E., Mena, O., Pan, S., Visinelli, L., Yang, W., Melchiorri, A., Mota, D. F., Riess, A. G., Silk, J. (2021), In the realm of the Hubble tension—a review of solutions, *Class. Quant. Grav.*, 38(15), 153001.
- Einstein, A. (1918), On gravitational waves, *Sitzungsberichte der Königlich Preussischen Akademie der Wissenschaften (Berlin)*, pp. 154–167.
URL: <https://einsteinpapers.press.princeton.edu/vol7-trans/25>
- Favata, M. (2010), The gravitational-wave memory effect, *Class. Quant. Grav.*, 27, 084036.
- Gasparotto, S., Vicente, R., Blas, D., Jenkins, A. C., Barausse, E. (2023), Can gravitational-wave memory help constrain binary black-hole parameters? A LISA case study, *Phys. Rev. D*, 107(12), 124033.

- Goldberger, W. D., Rothstein, I. Z. (2006), An Effective field theory of gravity for extended objects, *Phys. Rev. D*, 73, 104029.
- Goncharov, B., Donnay, L., Harms, J. (2024), Inferring Fundamental Spacetime Symmetries with Gravitational-Wave Memory: From LISA to the Einstein Telescope, *Phys. Rev. Lett.*, 132(24), 241401.
- Grant, A. M., Nichols, D. A. (2023), Outlook for detecting the gravitational-wave displacement and spin memory effects with current and future gravitational-wave detectors, *Phys. Rev. D*, 107(6), 064056. [Erratum: *Phys.Rev.D* 108, 029901 (2023)].
- Hoang, B.-M., Naoz, S., Kremer, K. (2020), Neutron Star–Black Hole Mergers from Gravitational-wave Captures, *Astrophys. J.*, 903(1), 8.
- Inchauspé, H., Gasparotto, S., Blas, D., Heisenberg, L., Zosso, J., Tiwari, S. (2024), Measuring gravitational wave memory with LISA, , .
- Isaacson, R. A. (1968), Gravitational Radiation in the Limit of High Frequency. II. Nonlinear Terms and the Effective Stress Tensor, *Phys. Rev.*, 166, 1272–1279.
- Maggiore, M. (2007), *Gravitational Waves. Vol. 1: Theory and Experiments*, Oxford University Press.
- Mastrogiovanni, S., Laghi, D., Gray, R., Santoro, G. C., Ghosh, A., Karathanasis, C., Leyde, K., Steer, D. A., Perries, S., Pierra, G. (2023), Joint population and cosmological properties inference with gravitational waves standard sirens and galaxy surveys, *Phys. Rev. D*, 108(4), 042002.
- Messenger, C., Read, J. (2012), Measuring a cosmological distance-redshift relationship using only gravitational wave observations of binary neutron star coalescences, *Phys. Rev. Lett.*, 108, 091101.
- Ni, W.-T., Zimmermann, M. (1978), Inertial and gravitational effects in the proper reference frame of an accelerated, rotating observer, *Phys. Rev. D*, 17, 1473–1476.
- O’Leary, R. M., Kocsis, B., Loeb, A. (2009), Gravitational waves from scattering of stellar-mass black holes in galactic nuclei, *Mon. Not. Roy. Astron. Soc.*, 395(4), 2127–2146.
- Peters, P. C., Mathews, J. (1963), Gravitational radiation from point masses in a keplerian orbit, *Physical Review*, 131(1), 435–439.
URL: <https://doi.org/10.1103/PhysRev.131.435>
- Poisson, E., Will, C. M. (2014), *Gravity: Newtonian, Post-Newtonian, Relativistic*, Cambridge University Press.
- Szabados, L. B. (2009), Quasi-Local Energy-Momentum and Angular Momentum in General Relativity, *Living Rev. Rel.*, 12, 4.
- Thorne, K. S. (1980), Multipole Expansions of Gravitational Radiation, *Rev. Mod. Phys.*, 52, 299–339.